Chapter 11

Sensing and Rheological Capabilities of MR Elastomers

Weihua Li, Tongfei Tian and Haiping Du

Additional information is available at the end of the chapter

http://dx.doi.org/10.5772/50501

1. Introduction

Magnetorheological elastomers (MREs) are smart materials where polarized particles are suspended in a non-magnetic solid or gel-like matrix. Two kinds of MREs, namely anisotropic and isotropic, are fabricated either under a magnetic field or without a field [1,2]. In anisotropic MREs, polarised particles are arranged in chains within a polymer media such as silicon rubber or natural rubber. The shear modulus of MRE can be controlled by the external magnetic field, which has led to many applications, such as tuned vibration absorbers, dampers and sensors [3].

Additives are used to adjust the mechanical properties or electrical performance of MREs. Silicone oil is an additive which is used to increase the gaps between the matrix molecules and to decrease the gaps between the conglutination of molecules. Apart from increasing the plasticity and fluidity of the matrix, the additives can average the distribution of internal stress in the materials, which makes them ideal for fabricating MRE materials. Graphite powder is a kind of additive which can affect the magnetorheology and electrical conductivity of MREs [4,5]. By introducing graphite microparticles into the elastic matrix, MREs exhibit a lower electrical conductive and a different magnetorheological response.

When the material in the matrix is magnetic, the polarization of the particles is less effective and the magnetorheological response is therefore smaller. The addition of magnetically active additives (other than MR particles) also decreases the magnetorheology [6, 7]. The overall properties of the elastomer composite are also influenced by the additives, as the filler material causes the volume to increase, so the previous effect also increases. Lokander et al. [7, 8] have shown that the absolute effect of MR (the difference between the zero-field modulus and modulus measured under an external magnetic field) is independent of the matrix material. However, the zero-field modulus can be much higher for hard matrix material

(for instance, where materials with high volume fraction of iron specifically possess a high zero-field modulus), which means that the relative magnetorheological effect is quite low.

MREs feature viscoelastic properties and magnetorheology [9]. The magnetorheology of MREs is described as a reversible change in modulus in an applied magnetic field. Aligned MREs have mostly been characterized at relatively low frequencies (1 to 20 Hz) to measure the changes in the dynamic shear modulus induced by the external magnetic field [9, 10]. Ginder et al. found a substantial magnetorheology over the entire frequency range studied. The increase in the shear modulus varied initially with the strength of the magnetic field but saturated at higher field strength. When the magnetic field was increased from 0 to 0.56 Tesla the consequent increase in shear modulus was nearly 2 MPa and the frequency of the resonance was shifted upward by over 20% [10]. Zhou et al. [9] stated that the changes of dynamic shear storage modulus can be over 50%, while Gong et al. [11] said that it can be over 100%. Lokander et al. studied the dynamic shear modulus for isotropic MR elastomers with different filler particles and matrix materials. They measured the magnetorheology as a function of the amplitude of strain and found that the magnetorheology decreases rapidly with increasing strain within the measured range, and is not dependent on the frequency of testing. The fact that the absolute magnetorheology is independent of the matrix material means that softer matrix materials will show a greater relative magnetorheology [7, 8].

The effect of additives on the sensing capabilities were studied by a few groups. Kchit and Bossis [7] found that the initial resistivity of metal powder at zero pressure is about 108 Ωcm for pure nickel powder and 106 Ωcm for silver coated nickel particles. The change in resistance with pressure was found to be an order of magnitude larger for a MRE composite than for the same volume fraction of fillers dispersed randomly in the polymer. Wang et al. [8] proposed a phenomenological model to understand the impedance response of MREs under mechanical loads and magnetic fields. Their results showed that MRE samples exhibit significant changes in measured values of impedance and resistance in response to compressive deformation, as well as applied magnetic field. Bica [9] found that MRE with graphite micro particles (~14%) is electroconductive. These MREs possess an electric resistance whose value diminishes with both the increase of the intensity of the magnetic field and with the compression force. Such a variation of resistance with magnetic field intensity is due to the compression of MRE with graphite microparticles. In the approximation of the perfect elastic body, the sums of the main deformations and the compressibility module of MRE with graphite microparticles, depend on the magnetic field intensity. Li et al. [10] introduced graphite into conventional MREs and found that a MRE sample with 55% carbonyl iron, 20% silicon rubber and 25% graphite powder exhibits the best performance. The test result showed that at a normal force of 5 N, the resistance decreases from 4.62 kΩ without a magnetic field to 1.78 kΩ at a magnetic field of 600 mT. The decreasing rate is more than 60%. This result also demonstrated the possibility of using MREs to develop a sensor for measuring magnetic fields. This result indicates that the detection is very sensitive to the normal force. When the normal force is 15N, the field-induced resistance only has less than 28% change from 0.65 kΩ at 0 mT to 0.47 kΩ at 600 mT.

Depending on an elasto-plastic asperity microcontact model for contact between two nominally flat surfaces, Kchit and Bossis developed a model to analyse the contact of two

rough surfaces. They used two kinds of magnetic particles: nickel and nickel coated with silver which are dispersed in a silicone polymer as the polarised particles [12]. To understand the complex conductivity of particle embedded composites, quantitative or semi-quantitative models can be used [16]. The Maxwell–Wagner and the Bruggeman symmetric and asymmetric media equations were introduced by McLachlan [17] to model the electrical behaviour of conductor-insulator composites. The microstructures for which these effective media equations apply are considered in simulating the measured impedance and modular spectra of these composites. Woo et al. [18] developed a universal equivalent circuit model in modelling the impedance response of composites with insulating or conductive particles or fibres. Based on the microstructure of MREs, Wang et al. proposed an equivalent circuit model to interpret the impedance measurement results [13].

This chapter is organized as follows. Section 2 describes the fabrication of graphite based MRE samples with various weight fractions. The morphology of the MRE samples and rheological properties of graphite based MREs were presented in Section 3 and 4, respectively. Section 5 presents the theoretical development based on a representative volume for investigating MRE electric properties. The main findings are summarized in Section 6.

2. Fabrication of graphite based MREs

The materials used for the Graphite based Magnetorheological Elastomers (Gr-MREs) are: silicone rubber (Selleys Pty. LTD), silicone oil, type 378364 (Sigma-Aldrich Pty. LTD), carbonyl iron particles, type C3518 (Sigma-Aldrich Pty. LTD) and graphite powder, type 282863 (Sigma-Aldrich Pty. LTD). The particle sizes of graphite powder are less than 20 μm, the iron particles' diameter is between 3 μm and 5 μm.

The MREs with various graphite weight fractions (Gr %) were fabricated to compare the effect of graphite on to MREs. Table 1 shows the compositions of all Gr MRE samples. all samples contain 10g carbonyl iron particles, 3g silicone rubber and 3g silicone oil. The only difference is the graphite weight fraction, which is from 0% to 23.81%. For each composition, the mixture is fabricated under a constant magnetic field of 165 mT to form anistropic MRE samples.

3. Microstructure observation

To see microstructure of Gr-MREs, LV-SEM (JSM 6490LV SEM) is used. Figures 1- 3 show the surface imaging for MRE microstructures. Specifically, Fig. 1 shows the microstructure of isotropic and anisotropic Gr-MREs without graphite. The carbonyl iron particles are arranged in chains in the anisotropic sample, where they are dispersed randomly in the isotropic sample. According to Fig. 2 (a) and Fig. 3 (a), in the anisotropic Gr-MREs, the carbonyl iron particles are arranged in chains, whereas the graphite powders dispersed randomly in the matrix. The reason of this phenomenon is that the magnetic field only affects the carbonyl iron particles, but not the graphite. So upon magnetisation, the carbonyl iron particle chains tend to orient along the same direction as the magnetic field in the matrix.

By comparing Fig. 1 (a), Fig. 2 (a) and Fig. 3 (ba), we can see that the carbonyl iron chains in the sample without graphite have the best alignment performance. Further, the carbonyl iron chains in Fig. 2 (a) are aligned better than those in Fig. 3 (a). The reason is that when the mixture of carbonyl iron, silicone rubber, silicone oil and graphite is curing under the magnetic field, the graphite powders in Gr-MREs affect the carbonyl iron particles' movement. The more graphite in the mixture, the more effects are applied on to the carbonyl iron chains, which influence the magnetorheology of MREs.

	Graphite based MREs							
Sample No.	1	2	3	4	5	6	7	8
Carbonyl iron	10g	10g	10g	10g	10g	10g	10g	10g
Silicone oil	3g	3g	3g	3g	3g	3g	3g	3g
Silicone rubber	3g	3g	3g	3g	3g	3g	3g	3g
Graphite	0g	1g	2g	3g	3.5g	4g	4.5g	5g
Graphite weight fraction (Gr %)	0%	5.88%	11.11%	15.79%	17.95%	20%	21.95%	23.81%

Table 1. Components of Gr MRE samples

4. MRE rheology

A rotational Rheometer (MCR 301, Anton Paar Companies, Germany) and a Magneto Rheolgical Device (MRD 180, Anton Paar Companies, Germany) were used to measure the MREs' mechanical properties. The Magneto Rheolgical Device is equipped with an electromagnetic kit which can generate a magnetic field perpendicular to the direction of the shear flow. Specifically, a 20mm diameter parallel-plate measuring system with 1 mm gap was used. The samples were sandwiched between a rotary disk and a base placed in parallel. In this study both a steady-state rotary shear and an oscillatory shear were applied for the experiments.

The schematic of the experimental setup is shown in Fig. 4. The stress and stain signals were output from two ports which were detected through a Data Acquisition (DAQ) board (Type: LABVIEW PCI-6221, National Instruments Corporation. U.S.A) and transferred to a computer by which the data was processed.

In this experiment the magnetic flux density of the sample of MRE (B_{MRE}) in the measuring gap depends not only on the current (I) applied to the samples, but also on the magnetic properties of MRE materials. The relationship between B_{MRE} versus I is found to be: $B_{MRE} = 220\,I$, where the units of B_{MRE} and I are in mT and Ampere (A), respectively.

In the following test, the test current varies from 0A to 2A with the increment 0.5A, for which the intensity of magnetic field is 0 mT to 440 mT with the increment 110 mT.

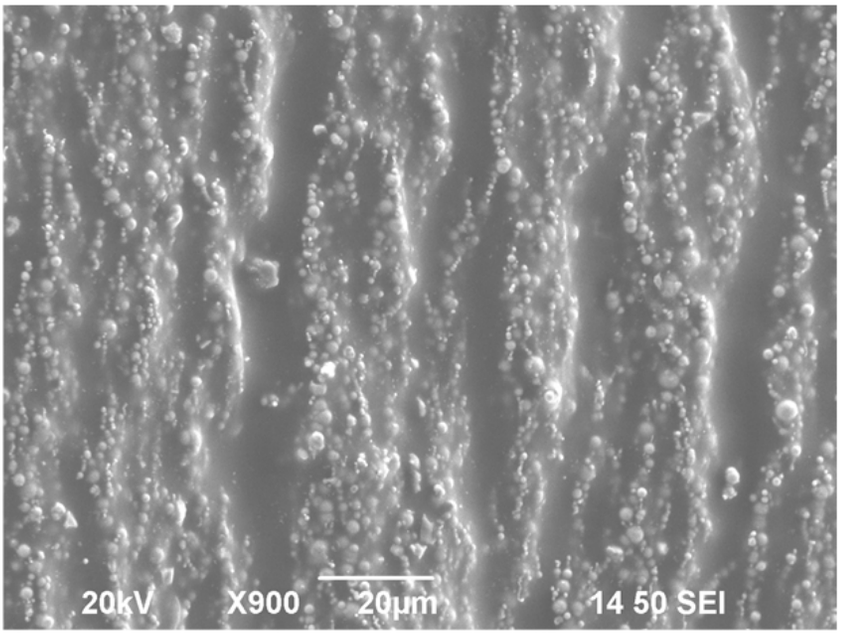

(a)

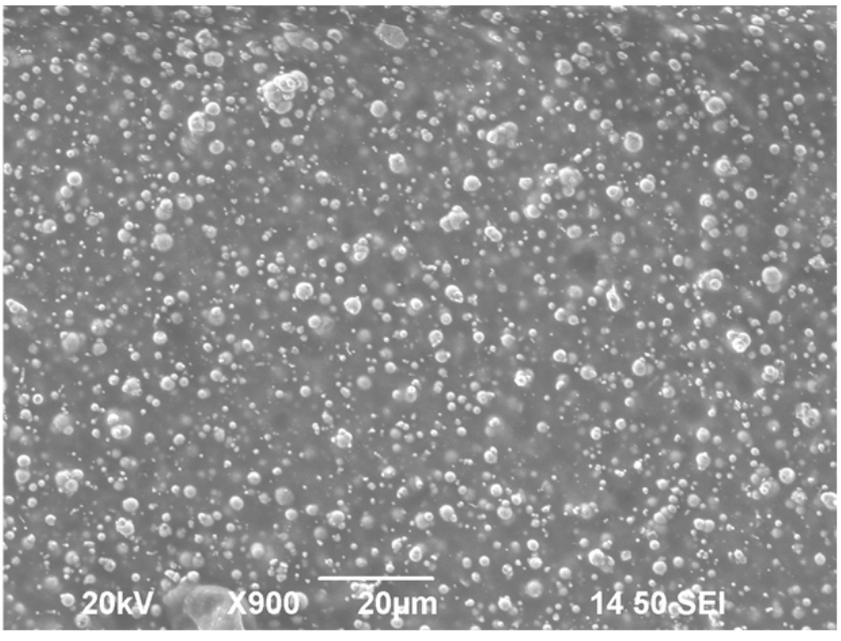

(b)

Figure 1. Microstructure of Gr-MREs (Gr 0%) (a) anisotropic (b) isotropic

4.1. Steady state results

Under rotary shear the shear stress and shear strain of MREs under fields varying from 0~440mT were measured. The MR effect was evaluated by measuring the shear strain-stress curve of the sample with and without a magnetic field applied.

Figures 5 and 6 show the strain-stress curve of different samples at 5 different magnetic field intensities ranging from 0 to 440mT.

The slope of the strain-stress curve is the shear modulus of the material. As can be seen in the figures, all the samples' shear modulus show an increasing trend with magnetic field before they reach magnetic saturation at high field strength, which proves that all the MRE samples exhibit obvious MR effects.

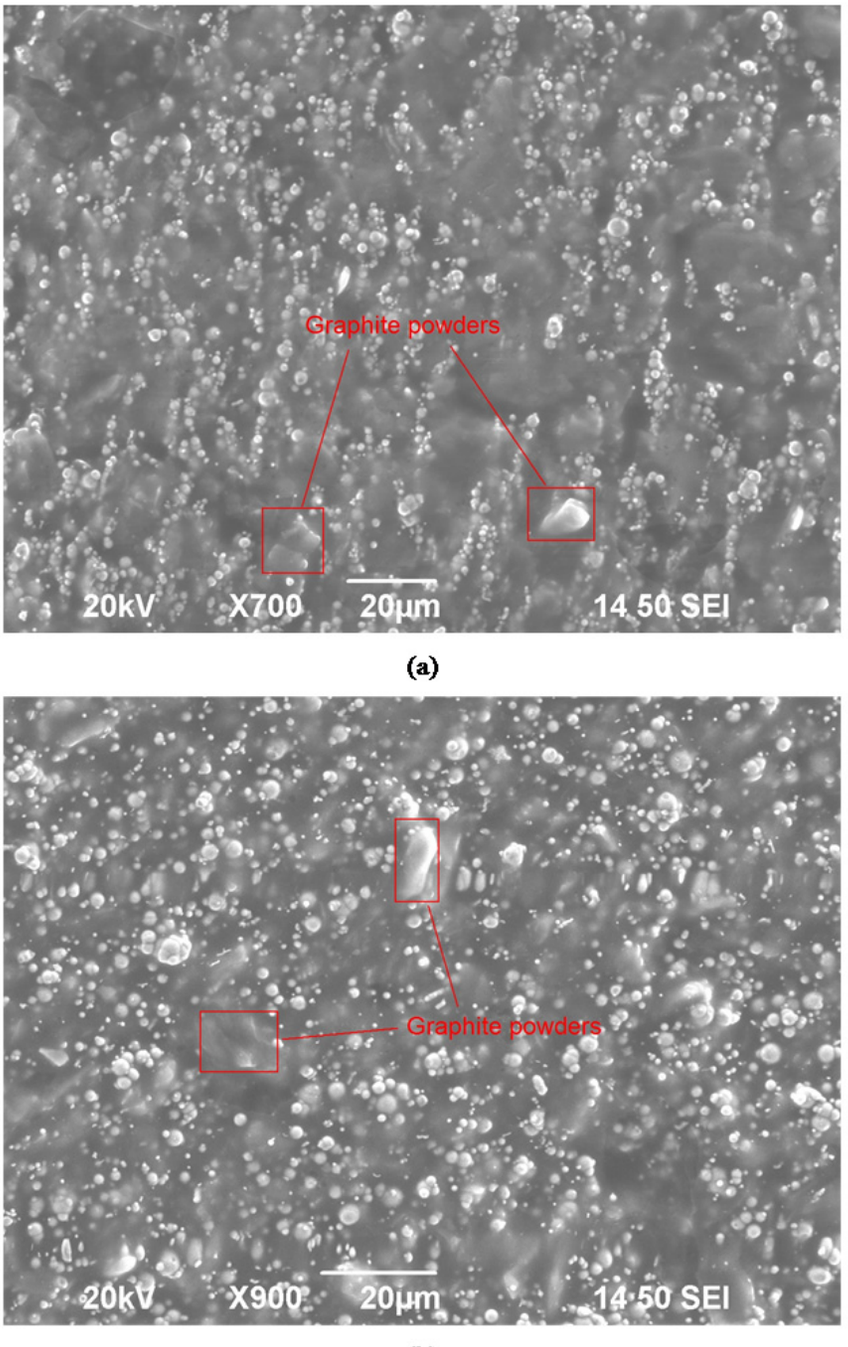

Figure 2. Microstructure of Gr-MREs (Gr 11.11%) (a) anisotropic (b) isotropic

From Figures 5 and 6, the shear stress shows a linear relationship with the shear strain when the strain is within a range. This means the MRE acts with linear viscoelastic properties when the strain is below a certain limit. For conventional MREs, the limitation is around

50% shear strain. When the graphite weight fraction increases from 0 to 15.79%, the range of linearity decreases from 50% to around 10%. For the samples with higher graphite weight fraction alike 23.81%, the linearity ranges are only 6% and 4% for isotropic and anisotropic samples, respectively. When the strain is above the limitation, the shear modulus reaches a saturation (maximum value) and decrease steadily. This could be due to sliding effect. The higher magnetic field intensity leads to higher steady shear stress. Fig. 7 shows the linear ranges of different samples at various magnetic field intensities.

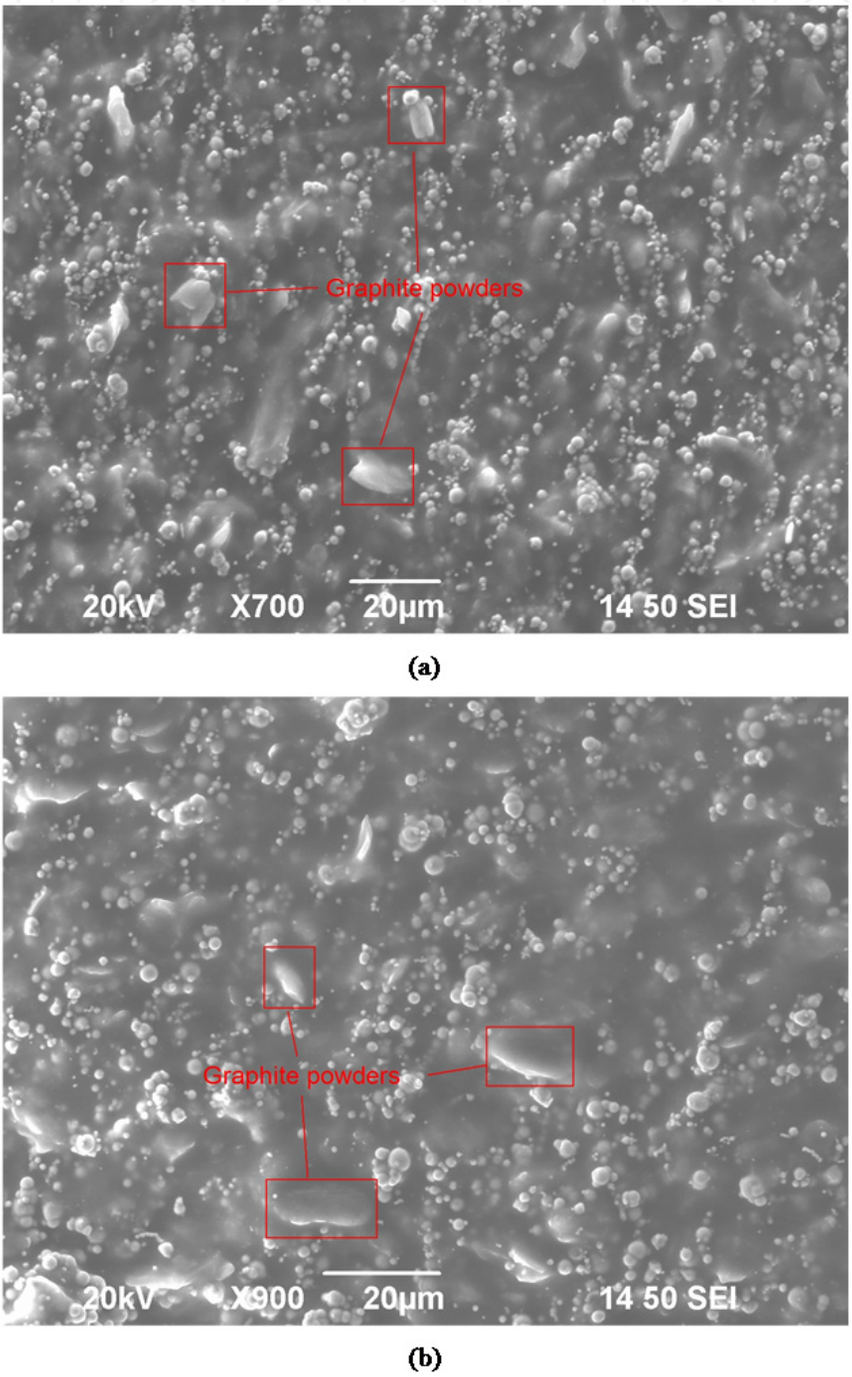

Figure 3. Microstructure of Gr-MREs (Gr 20%) (a) anisotropic (b) isotropic

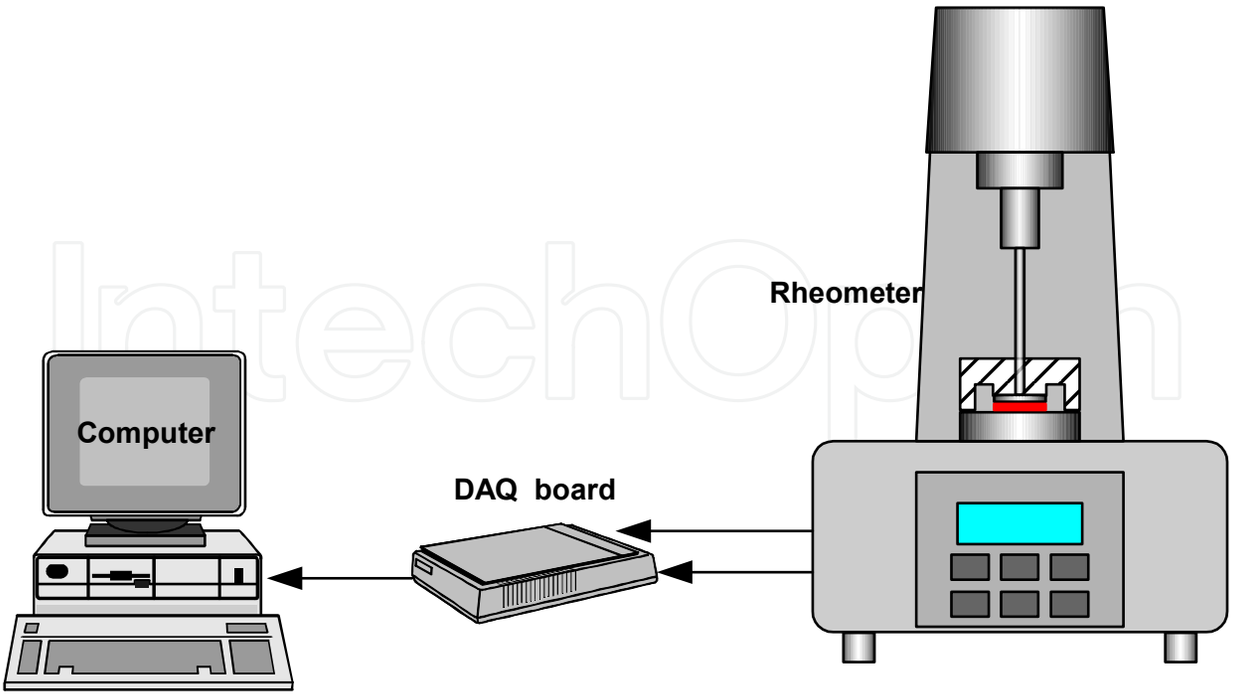

Figure 4. A diagram of the experimental setup

For the isotropic and anisotropic samples with same compositions, the isotropic samples always have the bigger linearity ranges and steady shear stress than chose of anisotropic samples.

For each curve, the slope equals the ratio between peak shear stress and relevant shear strain. By analyzing the slope of these curves, it is easy to see that the more graphite in the material, the smaller increment in slopes occurs when the magnetic field increase from 0 to 440mT. This is due to the contributions of graphite powders to the stiffness of the samples. The graphite increases the initial stiffness of Gr-MREs, thus the stiffness change induced by the MR effect can not be comparable to that conventional MREs. Fig. 8 shows the peak stresses of different samples for a magnetic field intensity equalling 220mT, 330mT and 440mT, respectively.

The relative MR effect ($\Delta G_{max}/G_0$) of several samples is shown in Fig. 9. G_0 denotes the MRE samples' zero-field modulus, ΔG_{max} denotes the saturated field-induced modulus, and $\Delta G_{max}/G_0$ denotes the relative MR effect.

It can be seen from Fig. 9 that G_0 is enhanced with the increase in graphite powders content. This result indicates that graphite powders can modify particle properties and, consequently, influenced the MR effect. From the abovementioned results, the exhibited MR effects correspond well with the microstructures of Gr-MREs.

4.2. Dynamic tests result

The dynamic mechanical behavior of MREs was studied by using the strain amplitude sweep tests. Five sets of data were collected for different amplitudes of oscillation, according

to various magnetic fields applied to the samples of MREs. Similar to the steady state tests, five different magnetic field intensities, 0, 110, 220, 330 and 440mT, were used in this experiment. A constant frequency of 5Hz was selected for the strain amplitude sweep tests.

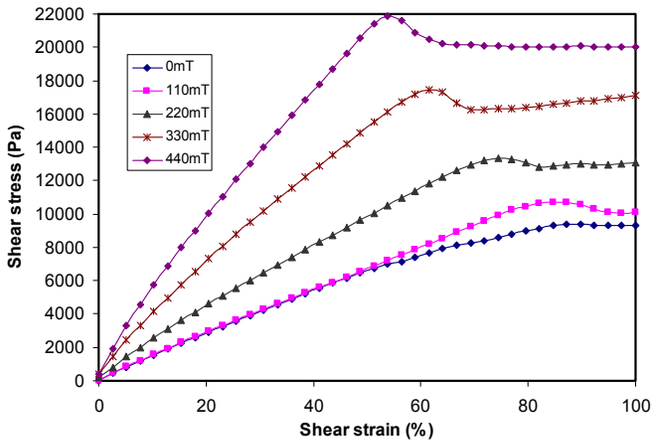

(a)

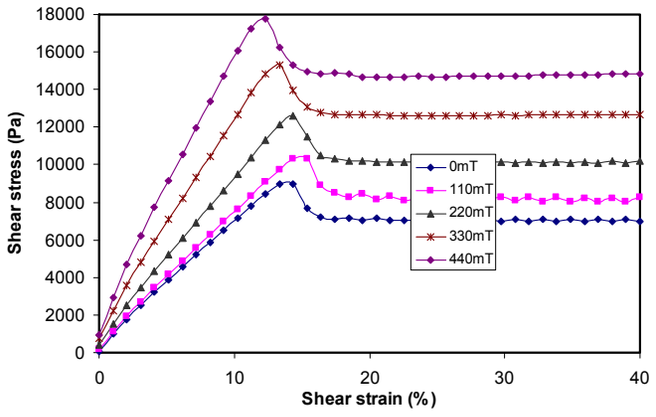

(b)

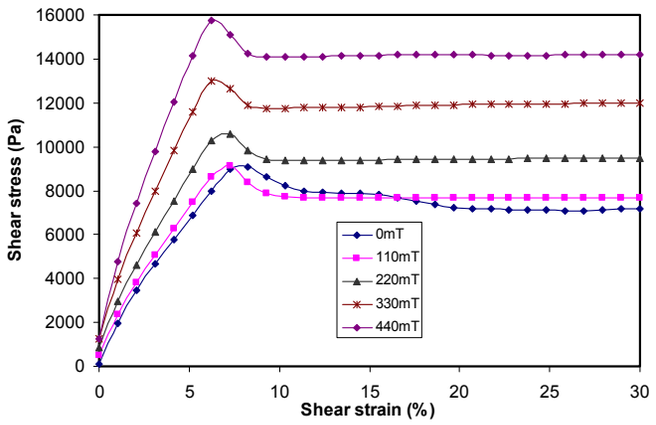

(c)

Figure 5. Strain-stress curve versus magnetic field (isotropic MRE) (a) Gr 0% (b) 15.79% (c) Gr 23.81%)

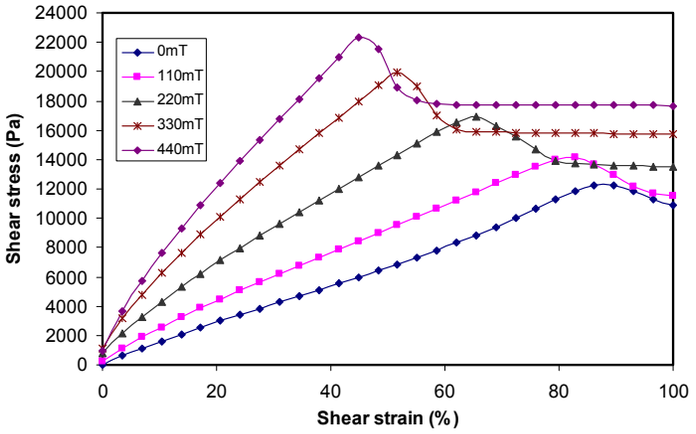

(a)

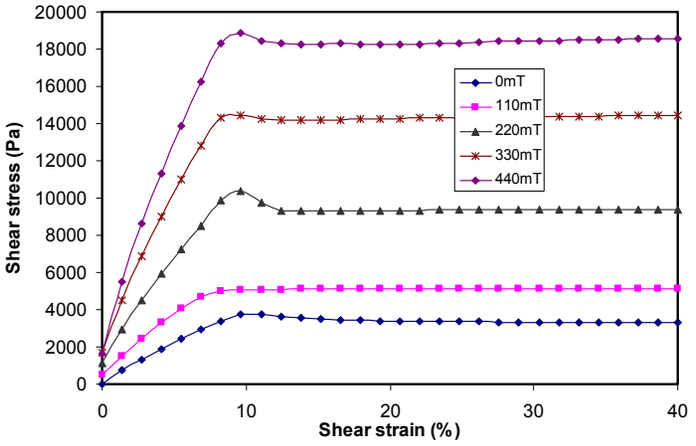

(b)

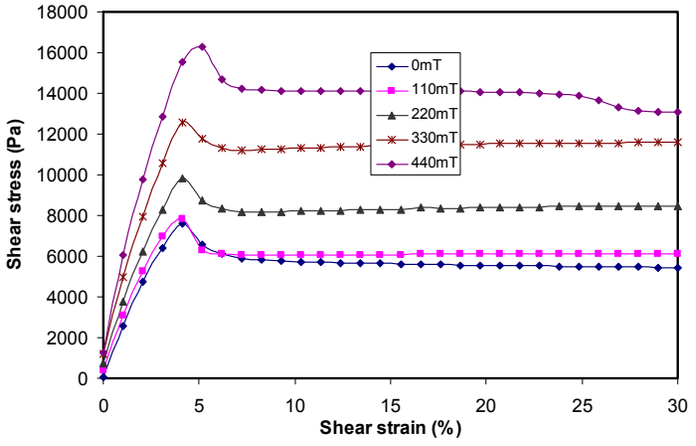

(c)

Figure 6. Strain-stress curve versus magnetic field (anisotropic MRE) (a) Gr 0% (b) 15.79% (c) Gr 23.81%)

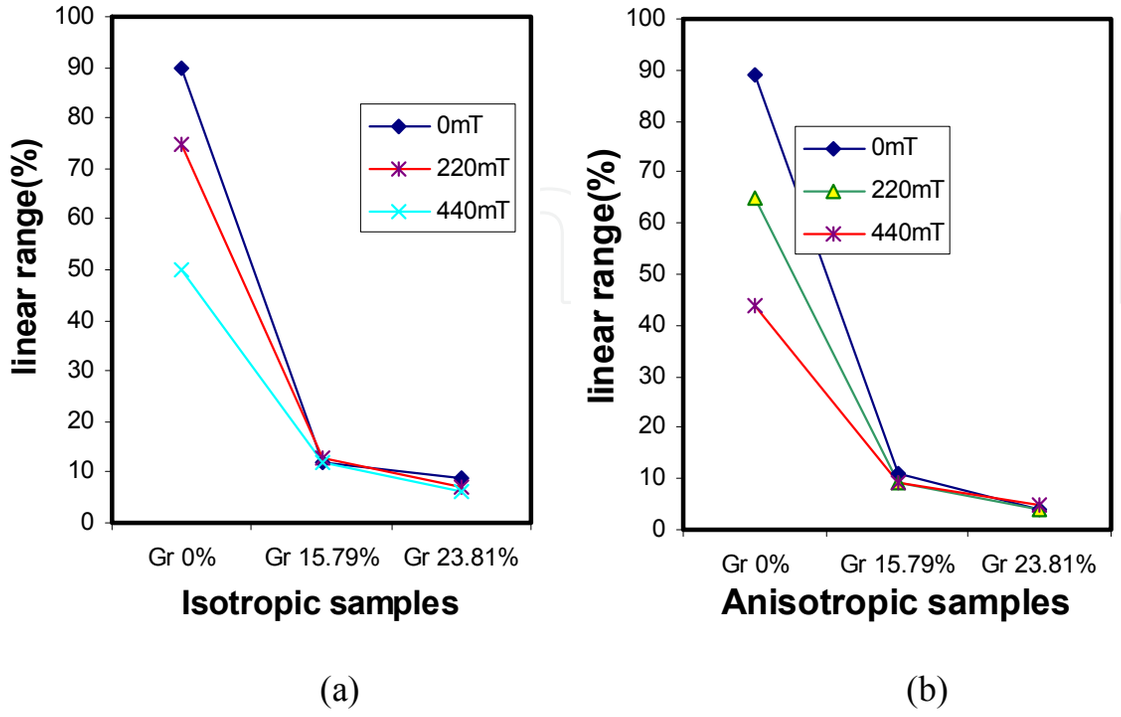

Figure 7. Linear ranges versus different samples (a) isotropic samples (b) anisotropic samples

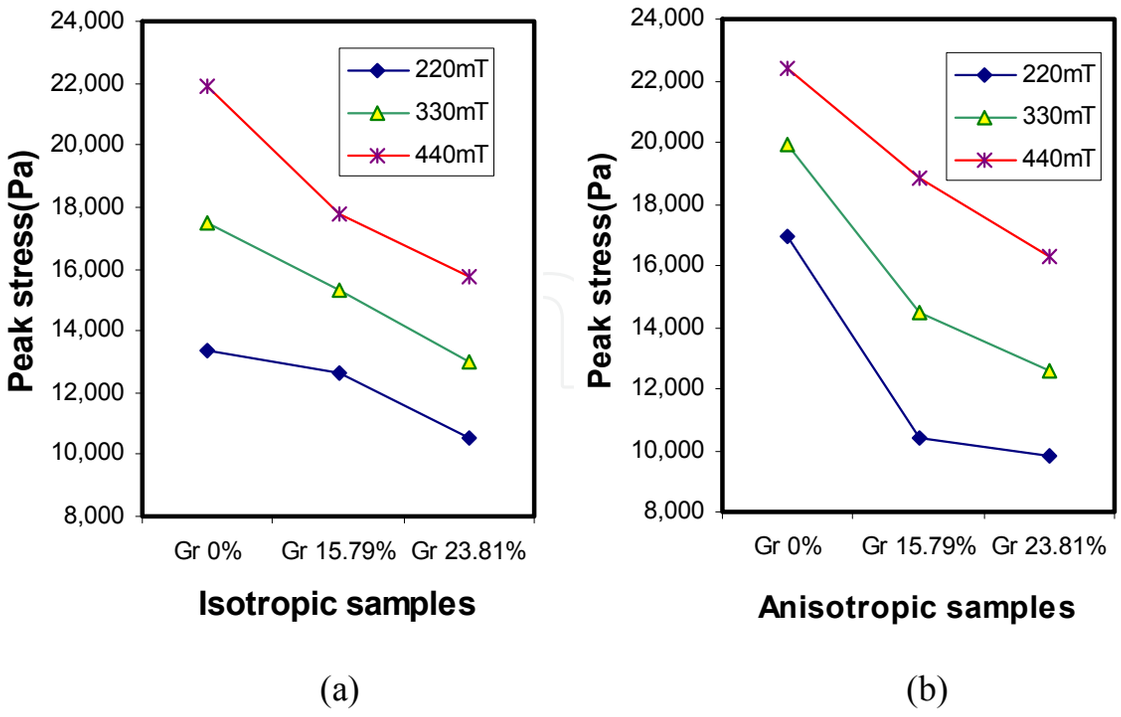

Figure 8. Peaks stresses versus different samples (a) isotropic samples (b) anisotropic samples

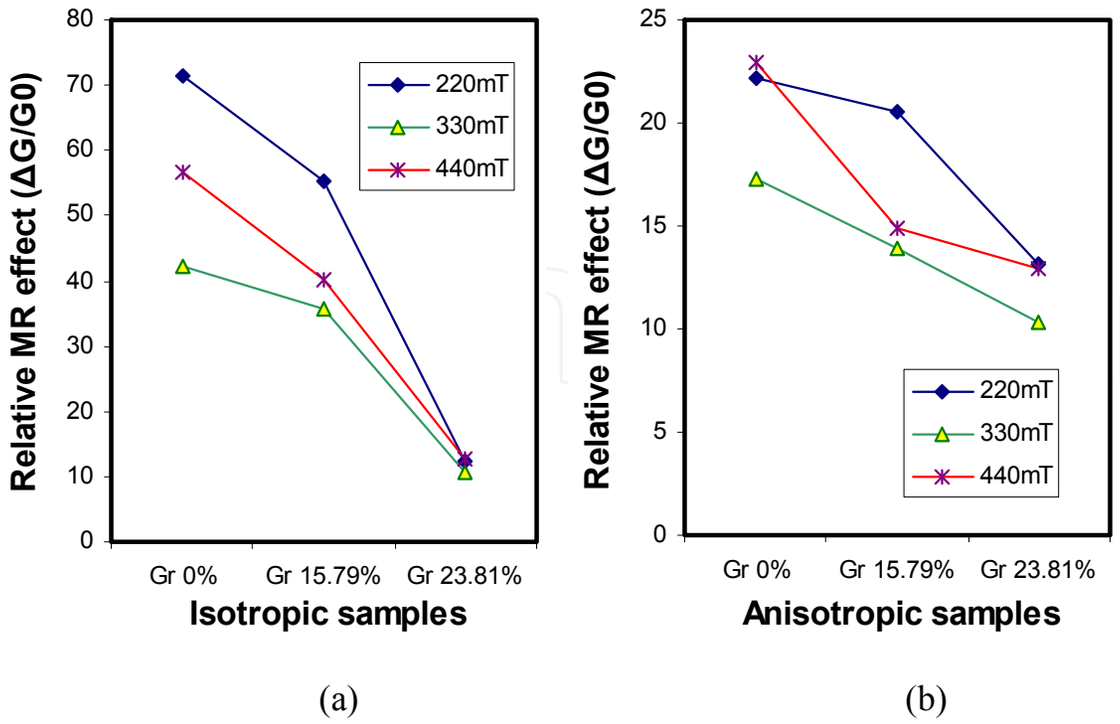

Figure 9. Relative MR effects versus different samples (a) isotropic samples (b) anisotropic samples

In the strain sweep test, the storage and loss moduli were measured by varying strain from 0.01% to 100% at different magnetic fields. Figs. 10-13 show the variation of storage and loss moduli with the strain amplitude sweep.

As shown in Figures from 10 to 13, the overall trend of storage modulus is decreasing with strain amplitude. The storage modulus goes down smoothly until 10% shear strain and begins to drop significantly beyond 10% shear strain. Except for isotropic MREs without graphite, the Loss modulus has almost the same trend as the storage modulus. This means that at the higher shear strains, the storage and loss moduli are much smaller than those at lower shear strains.

Figures 14 and 15 show the storage modulus of different samples at 0mT, 220mT and 440mT magnetic field. The data are collected at 10% and 87.5% shear strain, respectively.

As can be seen from Fig. 14, the storage modulus of all samples shows an increasing trend with graphite weight fraction at 10% shear strain which is in the linear range for most of the samples. In Fig. 15, it turns to a diminishing trend with graphite weight fraction at 87.5% shear strain which is out of the linear range. This means that in the linear range of shear strain, the samples with higher graphite weight faction have the bigger storage modulus.

Figures 16 and 17 show the storage modulus vs. magnetic field at 0.1% and 10% shear strain, respectively. The two shear strains are the beginning and the end of the linear range. From these figures we can see that the storage modulus shows an increasing trend with the intensity of magnetic field. The ratio of storage modulus at 440mT to that at 0mT is indicative of the MR effect. The MR effect of isotropic MREs with 0% graphite is around 4.5,

when the graphite weight fraction increases to 15.79% and 23.81%, the MR effect decreases down to around 2.8 and 2.8, respectively. For anisotropic samples, the MR effects of 0%, 20% and 23.81% Gr-MREs are 4.8, 3.2 and 2.2, respectively. This proves again that with the increase of graphite weight fraction, the MR effect decreases.

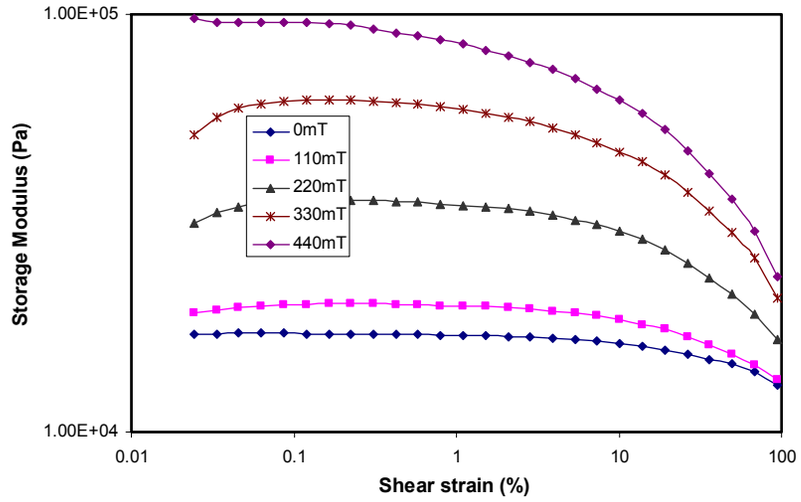

(a)

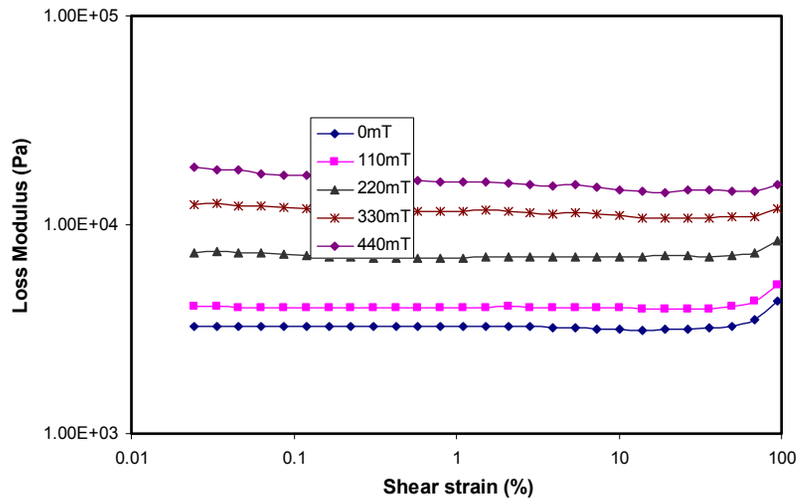

(b)

Figure 10. Storage and Loss Modulus versus strain amplitude sweep (isotropic MRE Gr 0%) (a) Storage modulus vs. shear strain (b) Loss modulus vs. shear strain

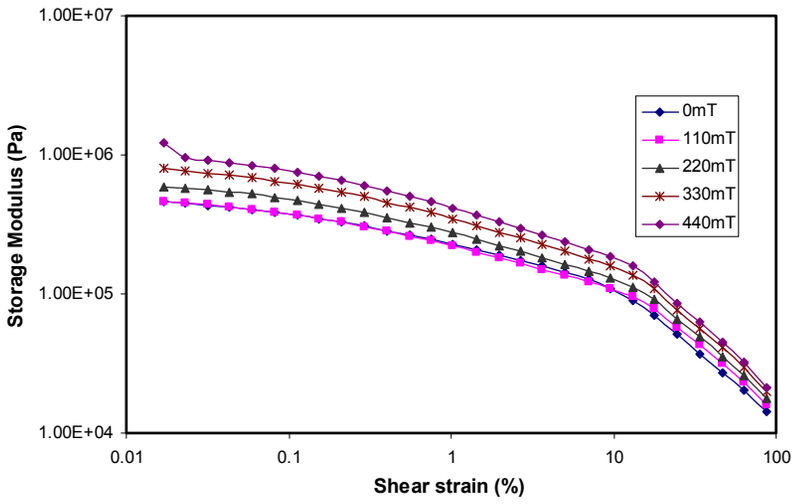

(a)

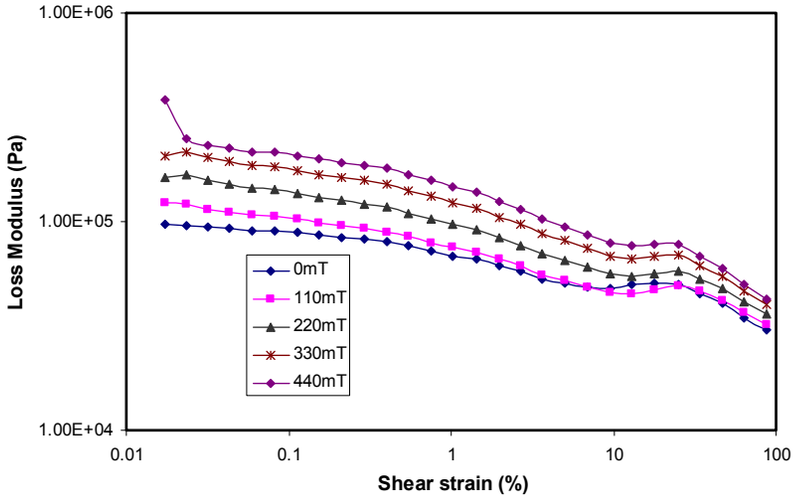

(b)

Figure 11. Storage and Loss Modulus versus strain amplitude sweep (isotropic MRE Gr 20%) (a) Storage modulus vs. shear strain (b) Loss modulus vs. shear strain

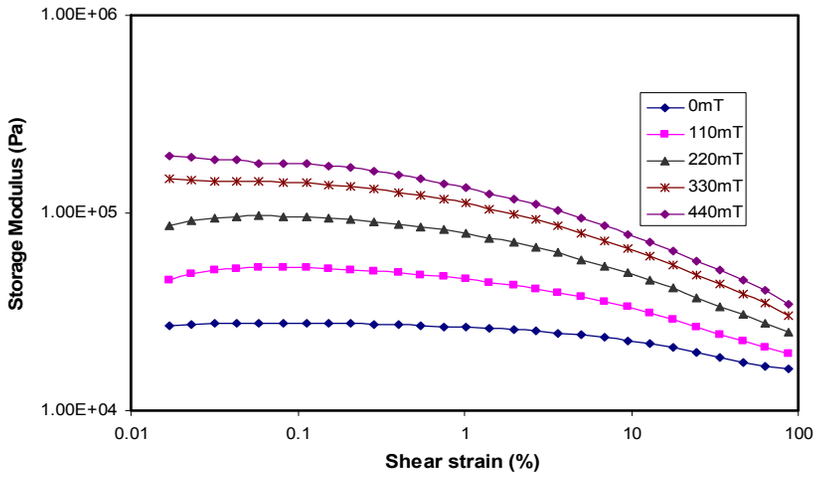

(a)

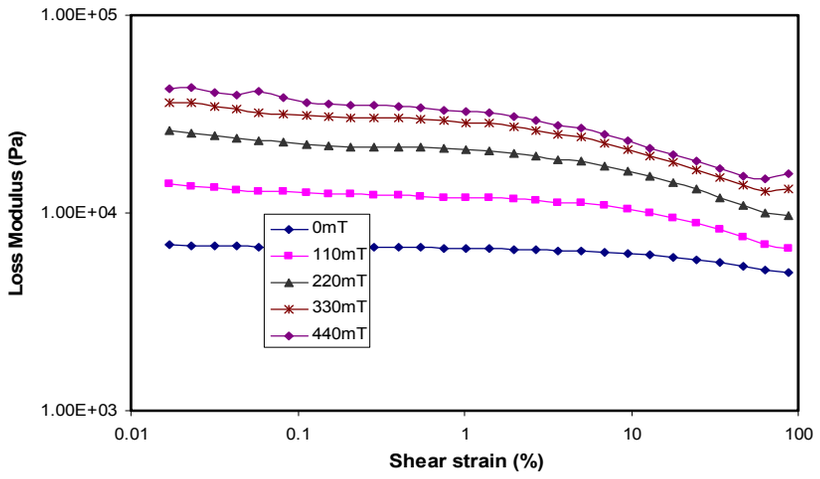

(b)

Figure 12. Storage and Loss Modulus versus strain amplitude sweep (anisotropic MRE Gr 0%) (a) Storage modulus vs. shear strain (b) Loss modulus vs. shear strain

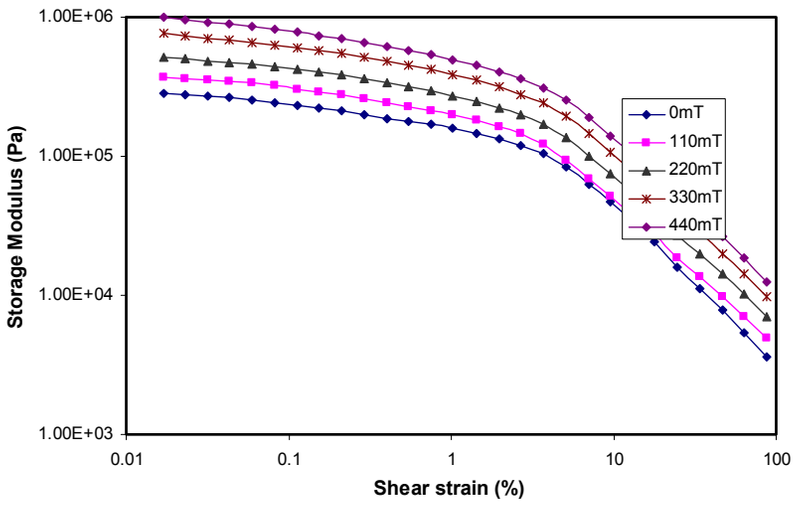

(a)

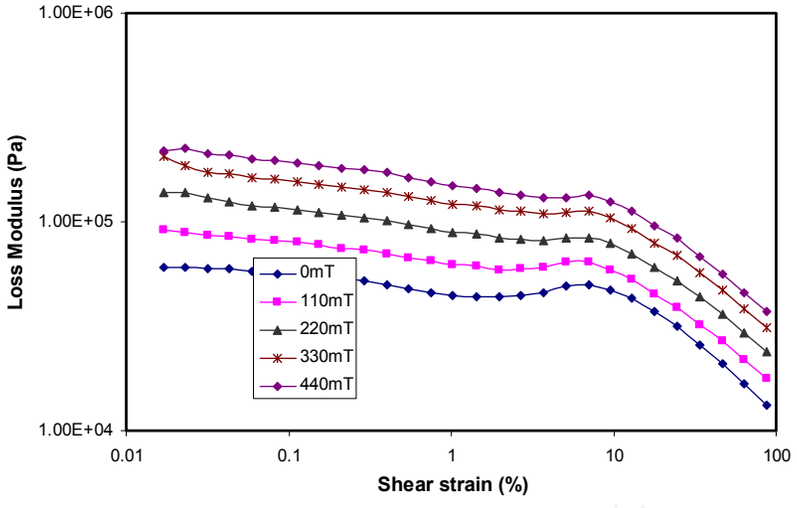

(b)

Figure 13. Storage and Loss Modulus versus strain amplitude sweep (anisotropic MRE Gr 20%) (a) Storage modulus vs. shear strain (b) Loss modulus vs. shear strain

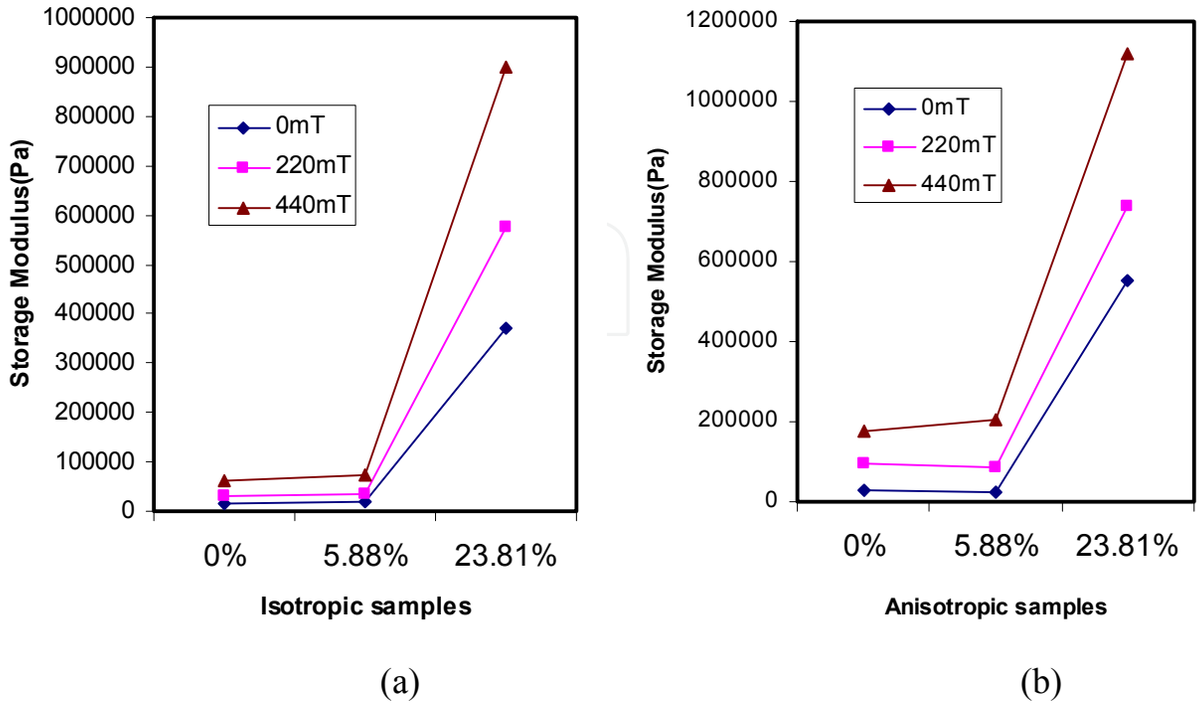

Figure 14. Storage Modulus of different samples at 10% shear strain (a) isotropic samples (b) anisotropic samples

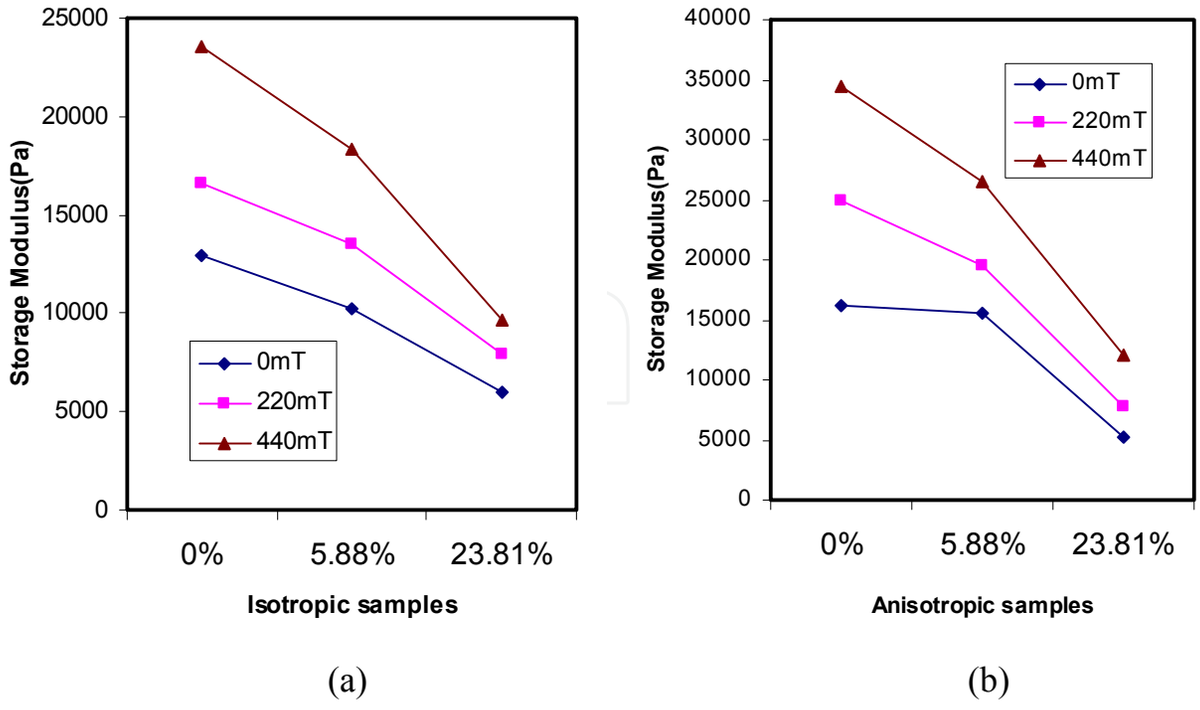

Figure 15. Storage Modulus of different samples at 87.5% shear strain (a) isotropic samples (b) anisotropic samples

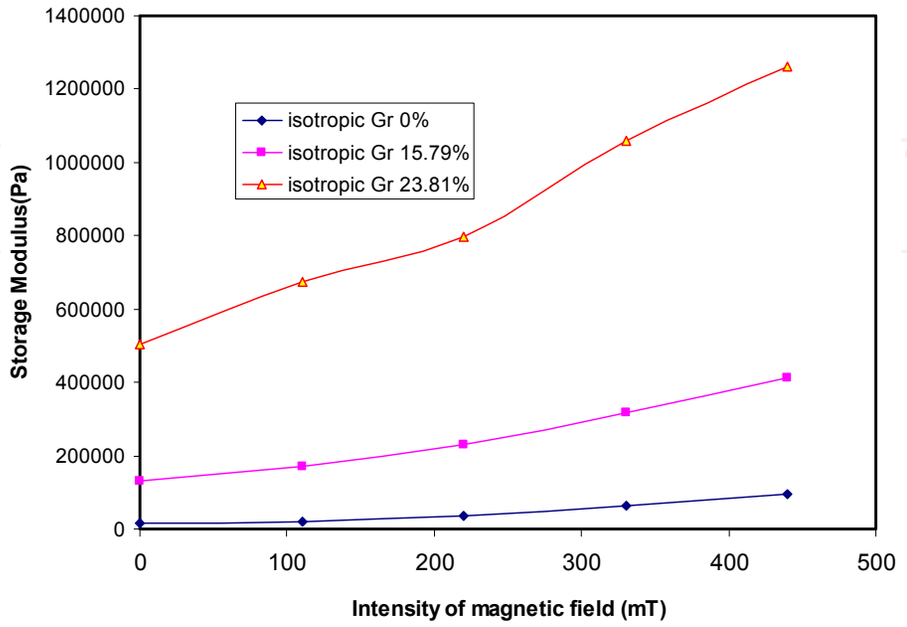

(a)

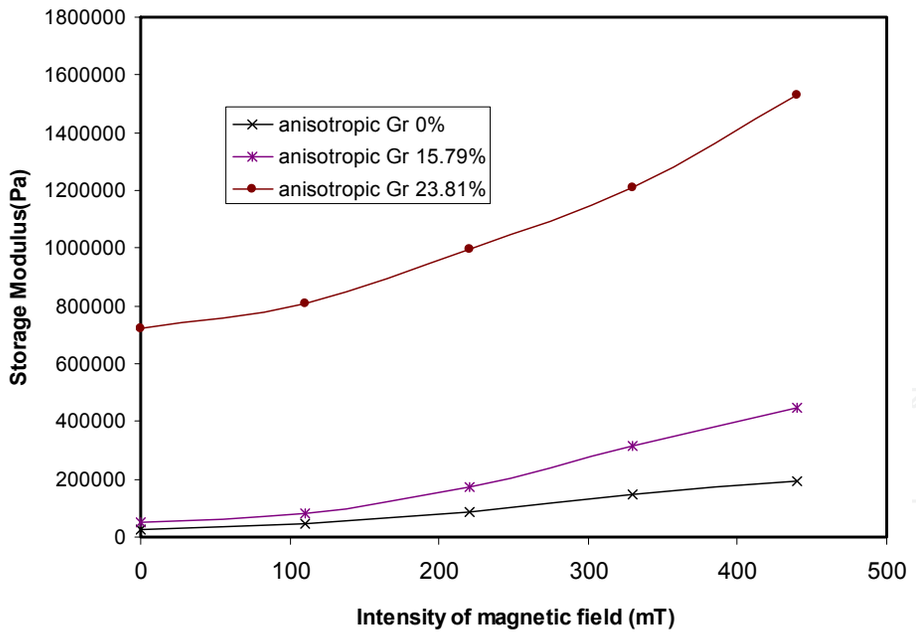

(b)

Figure 16. Storage Modulus versus magnetic field at 0.1% shear strain (a) isotropic samples (b) anisotropic samples

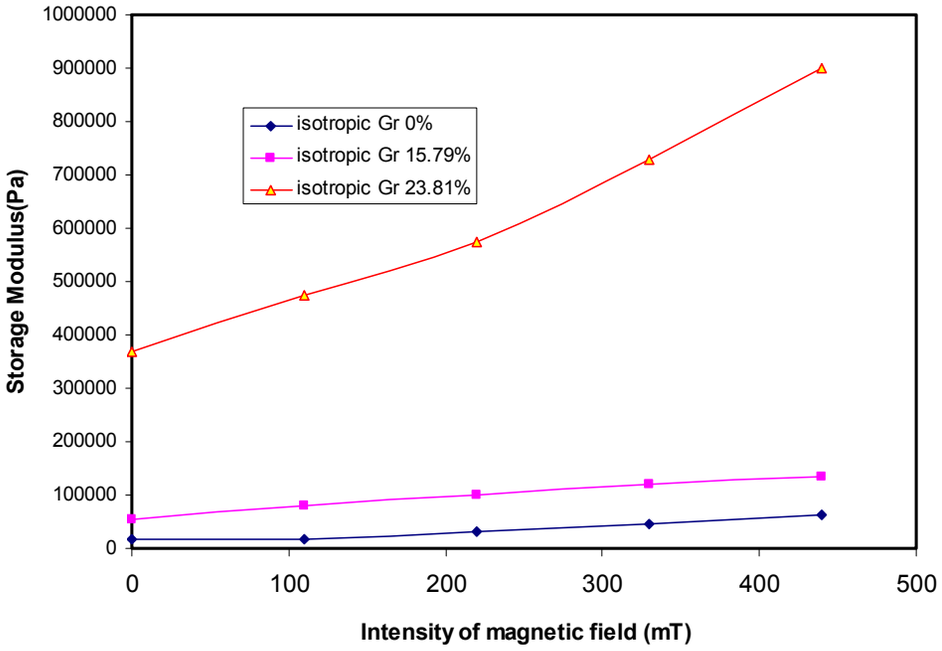

(a)

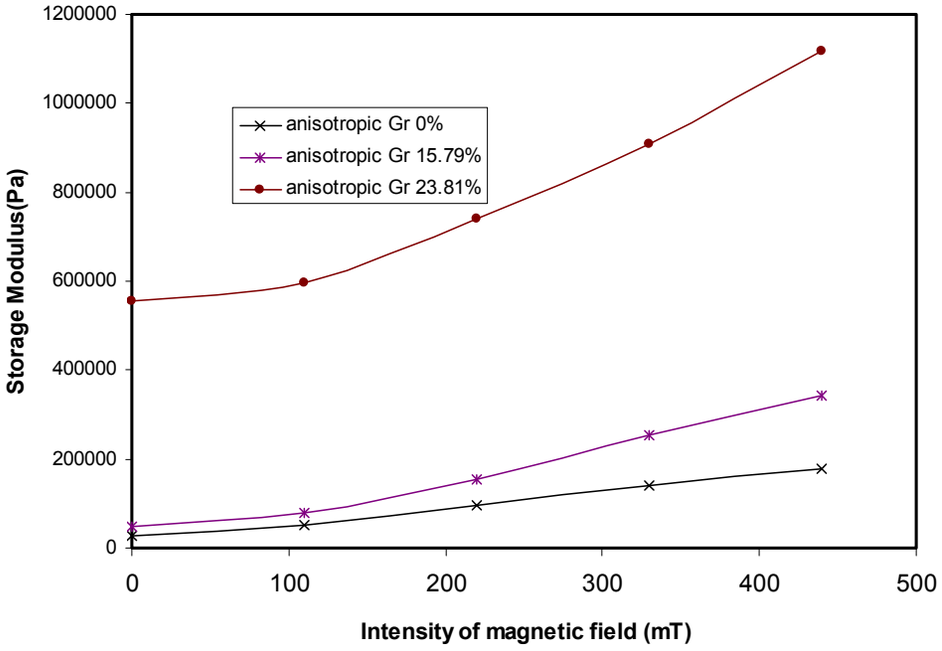

(b)

Figure 17. Storage Modulus versus magnetic field at 10% shear strain (a) isotropic samples (b) anisotropic samples

5. MRE sensing capabilities

5.1. Measurement of the relationship between the current and magnetic field

Figure 18 shows a schematic of the experimental device used. In this setup a long plastic plate is used to hold the weight which is applied load to the Gr-MRE samples. A Gaussmeter (HT201, Hengtong magnetoelectricity CO., LTD) is employed to test the intensity of the magnetic field. A multimeter (Finest 183, Fine Instruments Corporation) measures the resistance in the Gr-MRE samples.

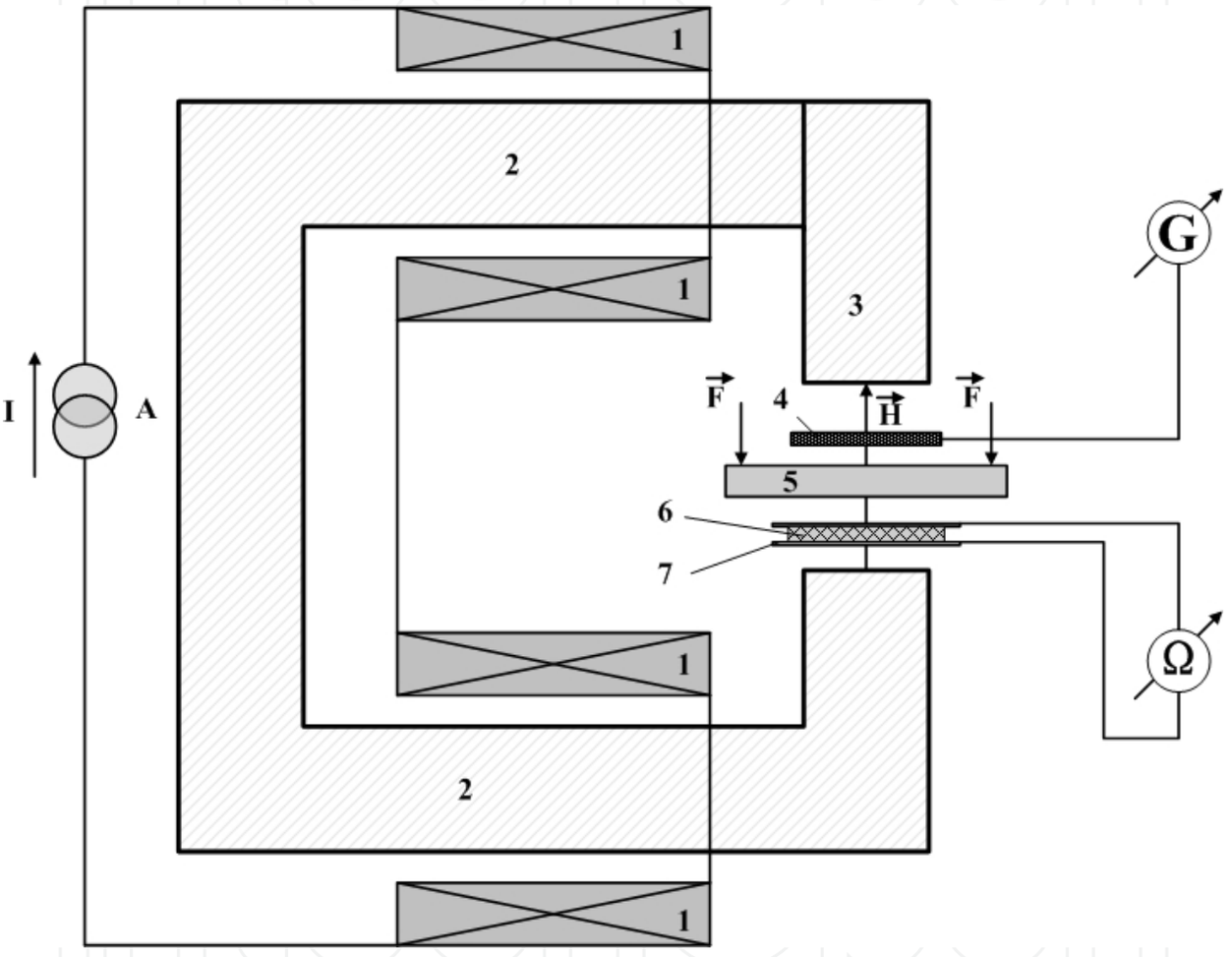

Figure 18. Sketch of the experimental device 1- coils; 2- electrical magnetic; 3- moving magnetic pole; 4- Gaussmeter probe; 5- plastic plate; 6- Gr MRE sample; 7- measuring copper plates; G- Gaussmeter; Ω- Multimeter; F- external force applied on Gr MRE samples

During the testing of the resistance of all the anisotropic MRE samples only the samples whose graphite weight fraction is higher than 15% are detectable by Finest 183 multimeter. Thus, among the tested anisotropic MRE samples only three of them are considered in Table 1, namely those whose graphite weight fractions are 20%, 21.95% and 23.81%. The results of these tests are shown in Figures 19, 20, and 21, respectively for the following data of anisotropic MRE with graphite weight fraction 20%, 21.95% and 23.81%.

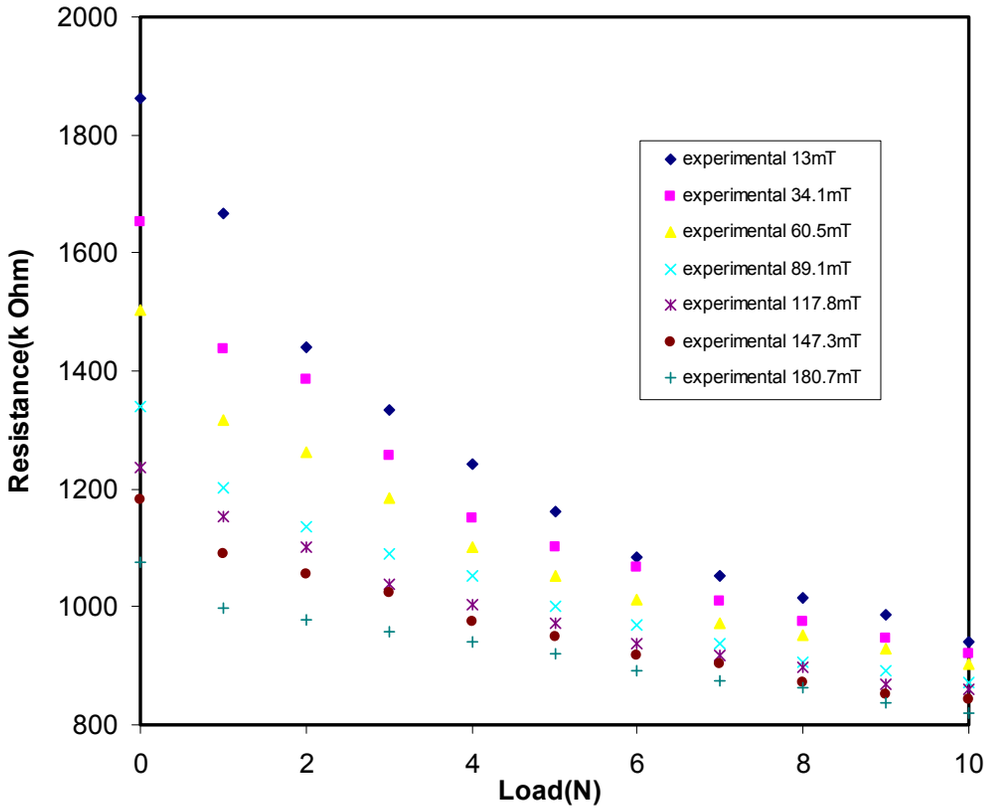

Figure 19. Resistance versus load (anisotropic MRE Gr 20%)

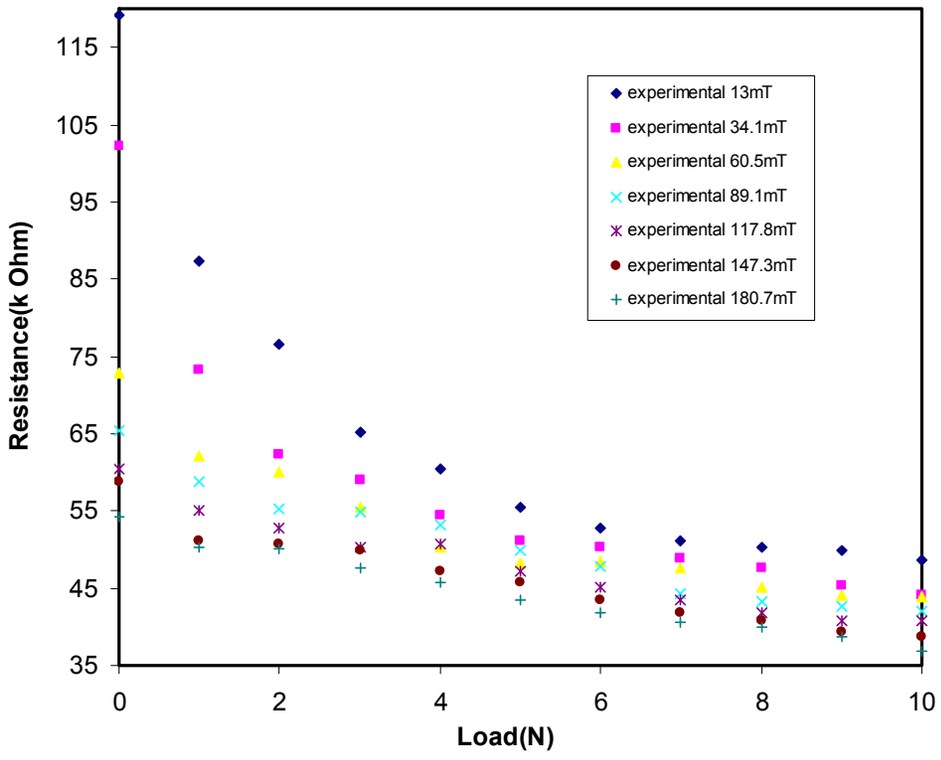

Figure 20. Resistance versus load (anisotropic MRE Gr 21.95%)

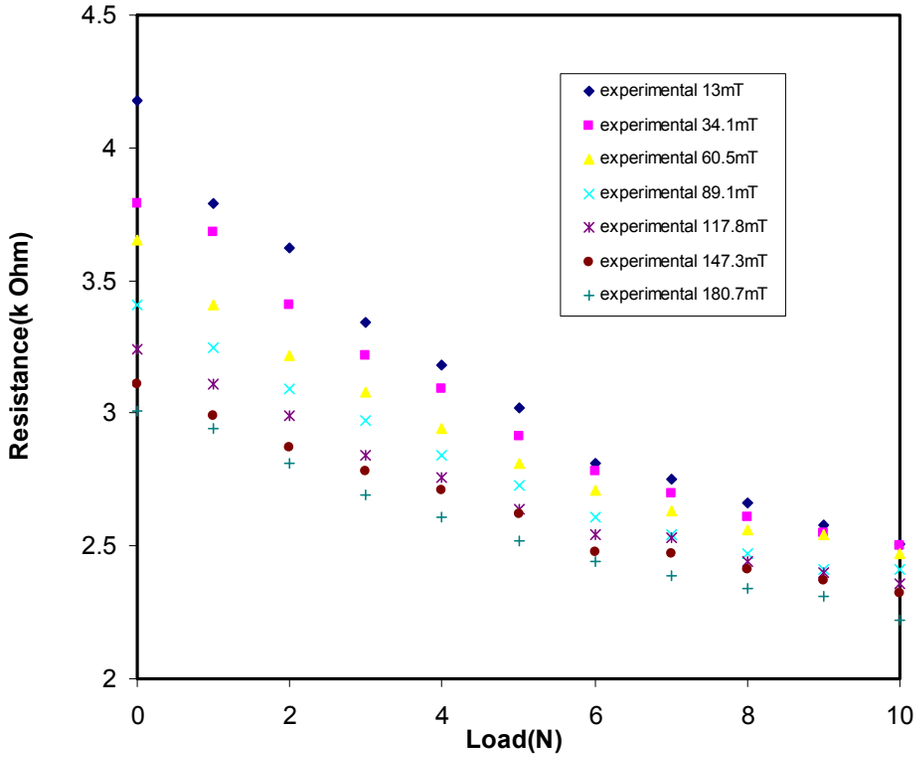

Figure 21. Resistance versus load (anisotropic MRE Gr 23.81%)

As shown in the plots similar trends are observed for the three samples. Specifically, in a fixed magnetic field, when the external load increases from 0 to 10 N, the resistance reduces in all three samples. With small loads, the resistance changes significantly but it decreases slowly when the load is more than 5 N. According to the absolute values, the sample with higher graphite weight fraction shows the higher electrical conductivity and the smaller decline in resistance. For instance, the resistance of the sample with graphite weight fraction 20% drops from 1862 kΩ at 0 N to 942 kΩ at 10 N, whereas a decline from 4.18 kΩ at 0 N to 2.51 kΩ at 10 N for the sample with graphite weight fraction 23.81%.

Besides, the resistance of each sample at a fixed external load decreases with increase in magnetic field intensity. Considering the sample with 21.95% graphite weight fraction as an example, at 5 N external force, the resistance 55.4 kΩ without the magnetic field decreases to 43.5 kΩ at a 440 mT magnetic field. This trend is shown in detail in Fig. 22.

5.2. A representative volume unit based mathematical model for investigating the magnetic field dependent sensing capabilities

5.2.1. Theoretical approach

From the Dipole Model a Representative Volume Unit (RVU) is derived. A RVU consists of two neighbouring hemispheres and the surrounding polymer matrix, which can be regarded as the minimum volume element in the conventional MRE. Fig. 23 shows the position of RVU in carbonyl iron particle chains and a longitudinal section of the unit is shown in Fig. 24.

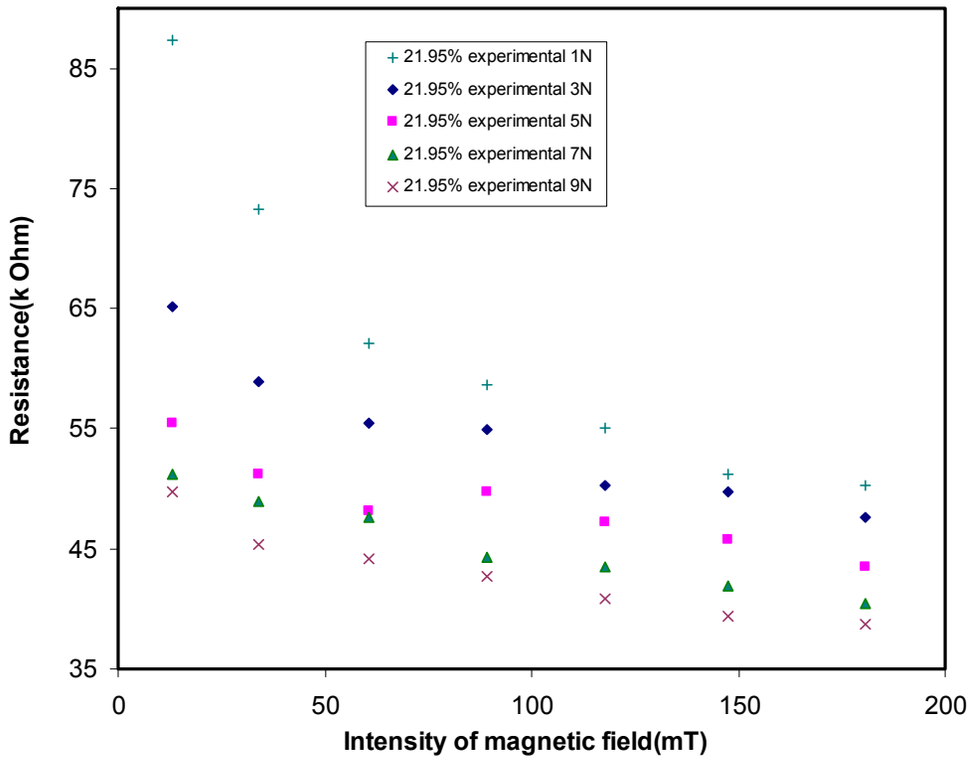

Figure 22. Resistance versus magnetic field (anisotropic MRE Gr 21.95%)

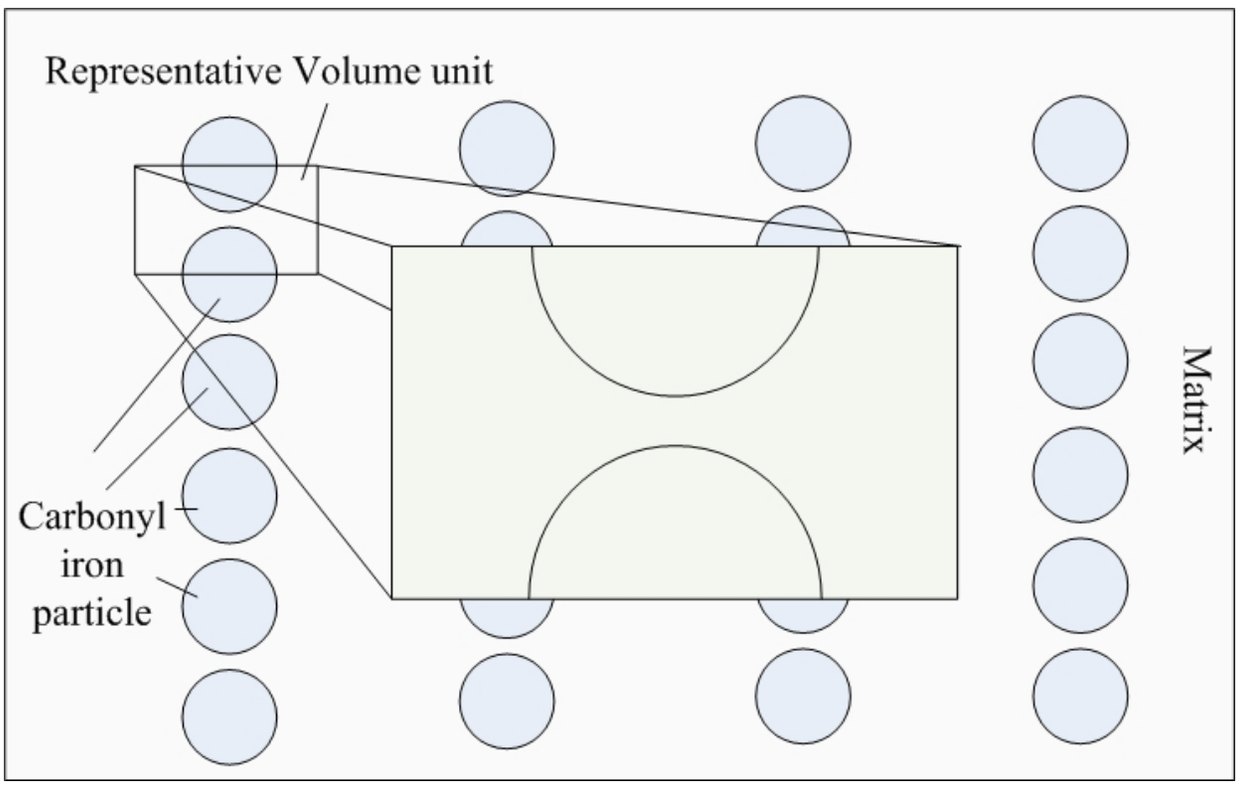

Figure 23. RVU in carbonyl iron chains

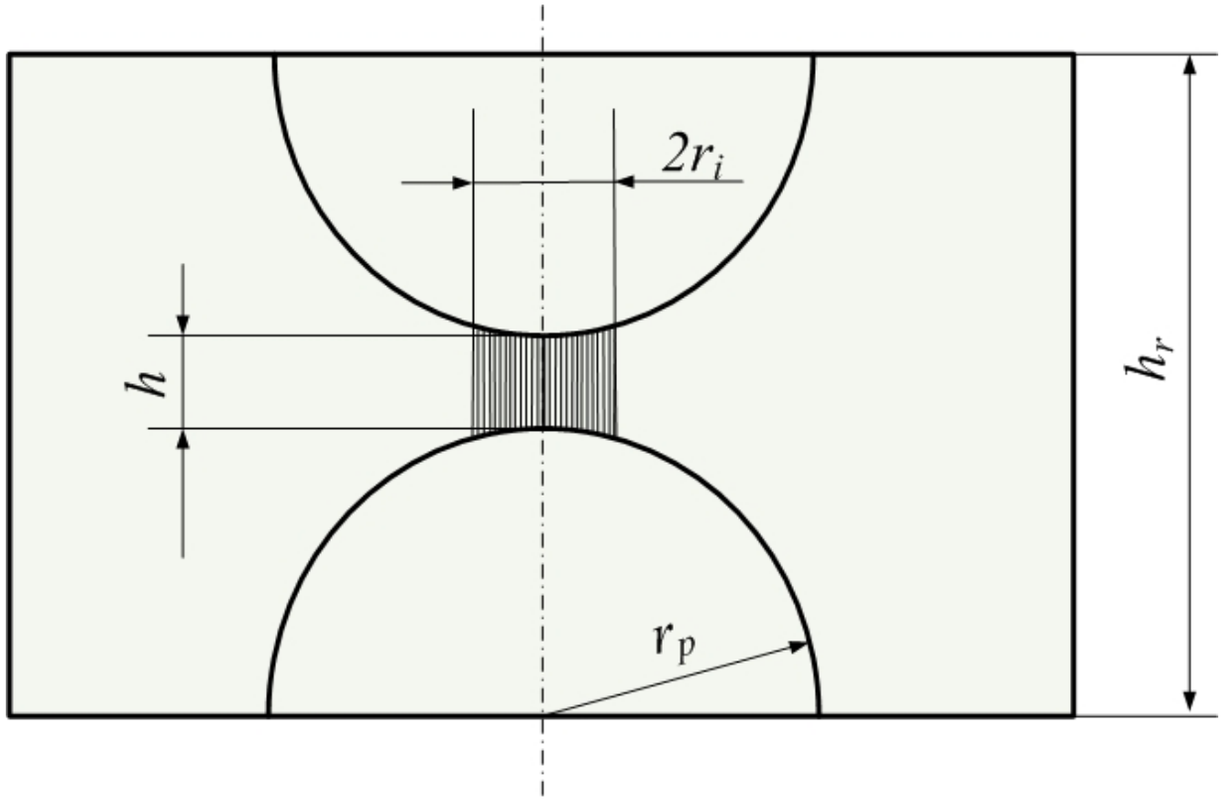

Figure 24. The longitudinal section of RVU

The RVU is a model for ideal anisotropic MREs which is supposed to have a chain structure.

Given the iron particle volume fraction ϕ in the RVU, the area of cross section can be expressed as

$$S_r = \frac{V_r}{h_r} = \frac{V_s}{\phi h_r} = \frac{4\pi r_p^{\,3}}{3\phi\left(2r_p + h\right)} \approx \frac{2\pi r_p^{\,2}}{3\phi} \tag{1}$$

where ϕ is the iron particle volume fraction, r_p is the particle radius, h is the particle distance, h_r is the distance between two half spheres, V_s is the particle volume, V_r is volume between two particles, and S_r is the cross section area.

In the RVU, the conductivity of the iron particles is much higher than that of the polymer, therefore the electric potential drops within the particles can be neglected. Due to system geometry and electrical properties, most of the current flowing through the RVU concentrates on the small area between the two adjacent hemispheres. Specifically, given the intensity of current flowing through the polymer is E, the intensity of the local electric field is

$$E_{loc} = \frac{h_r E}{h} = \frac{(2r_p + h)E}{h} \approx 2r_p \frac{E}{h} \tag{2}$$

Owing to the magnetic attraction during MRE preparation, the insulating polymer film between two neighbouring iron particles (here described by h) is very thin, and it is across

this film that the electrical field induced tunnel current can occur. The Fowler-Nordheim equation [19-21] can be used to express the tunnel current. In addition, the iron particles dispersed in the polymer matrix contribute to the conductivity of the polymer and then the total current density is the sum of the tunnel density j_t and the conduction density of the polymer j_c

According to the Fowler-Nordheim equation, the relation between the tunnel density j_t and electric field intensity E is

$$j_t = \alpha E_{loc}^2 \exp\left(-\frac{\beta}{E_{loc}}\right) \tag{3}$$

in which α and β are constants determining the tunnel current. So the total current density j is

$$j = j_t + j_c = \alpha E_{loc}^2 \exp\left(-\frac{\beta}{E_{loc}}\right) + \sigma_f E_{loc} \tag{4}$$

in which σ_f is the conductivity of the polymer film.

The total current density j is for the current flowing through the small area between the tips of two adjacent iron particles, however, the overall density of RVU j_r should be derived from its entire cross section. So from the total density of RVU j_r and the electric field intensity E, the global conductivity of typical MRE σ_r can be represented as

$$\sigma_r = \frac{j_r}{E} = \frac{\pi \cdot r_i^2 \cdot j}{S_r \cdot E} = 3\phi \cdot r_i^2 \left[\frac{2\alpha}{h^2} E \exp\left(-\frac{h\beta}{2r_p E}\right) + \frac{\sigma_f}{r_p h}\right] \tag{5}$$

in which r_i is the radius of the circular section across which the tunnelling current flow, as shown in Fig. 24.

MRE also exhibits piezoresistivity. When a MRE sample is compressed, its conductivity increases. This phenomenon is explained by two factors, one of which is the increments of the conductive area induced by the deformation of MREs and the other is the reduction of the thickness of the polymer membrane between the two adjacent iron particles. Because of the large ratio of r_i/h, it is difficult to compress the membrane further and thus the increment of the conductive area is the significant reason for the conductivity increasing.

From the Hertz Theory [22-24], when the initial pressure applied on MRE is σ_0 through a constant loading, corresponding to which there is an initial contact area radius r_{i0}

$$r_{i0} = \left[\frac{3\pi\sigma_0\left(1-\nu^2\right)}{2E_p}\right]^{1/3} \cdot r_p \tag{6}$$

Where ν is the Poisson's ratio, E_p is the Young's Modulus.

So the radius r_i increases along with the increment of pressure

$$r_i = r_{i0} + r_p\left(\left(\sigma_0 + \sigma\right)^{1/3} - {\sigma_0}^{1/3}\right)\cdot\left(\frac{3\pi\left(1-\nu^2\right)}{2E_p}\right)^{1/3} \tag{7}$$

The magnetic field also contributes to the electrical resistance of MREs. When the external magnetic field is applied to MREs, the carbonyl iron particles are attracted by the poles of magnetic field, with closer magnetic pole providing more powerful magnetic force than the other pole. So the attraction from the farther magnetic pole can be neglected.

For the two iron particles in each RVU, the magnetic attraction from the pole applied to the farther particle compresses the thin film between the two adjacent iron particles. Similar to the piezoresistivity, the increment of the conductive area is the main cause for the conductivity increasing.

Thus, the radius r_i can be updated as

$$r_i = r_{i0} + r_p\left(\left(\sigma_0 + \sigma_1 + \sigma_2\right)^{1/3} - {\sigma_0}^{1/3}\right)\cdot\left(\frac{3\pi\left(1-\nu^2\right)}{2E_p}\right)^{1/3} \tag{8}$$

in which, σ_1 is the stress due to pressure, σ_2 is the stress from the magnetic attraction.

So the dependence of the conductivity of MREs on electric field intensity and the stress due to pressure is

$$\sigma_m = 3\phi\cdot\left[\frac{2\alpha}{h^2}E\exp\left(-\frac{h\beta}{2r_pE}\right)+\frac{\sigma_f}{r_ph}\right]\cdot\left[r_{i0} + r_p\left(\left(\sigma_0 + \sigma_1 + \sigma_2\right)^{1/3} - {\sigma_0}^{1/3}\right)\cdot\left(\frac{3\pi\left(1-\nu^2\right)}{2E_p}\right)\right]^2 \tag{9}$$

When the initial condition σ_0 and r_{i0} are set, Apart from E and σ, the other parameters in this equation are all constants. So the conductivity of MREs σ_m is dependent on the intensity of the electric field E and the stress due to pressure σ.

In response to the effects of graphite and carbonyl iron on the resistance model, two parameters λ_g and λ_i are introduced to show the effects of graphite volume fraction ϕ_g and carbonyl iron volume fraction φ_i to the conductivity of new MREs. Two parameters λ_g and λ_i show the contribution of the carbonyl iron particles and graphite powder to the resistance respectively. The higher are values for λ_g and λ_i, the less resistance the Gr-MREs have.

In the RVU, the iron particle volume fraction is set as ϕ = 0.4, which means that the volume of two hemispheres is 40% of the whole volume of RVU.

The shape of Gr MRE samples is fixed. The thickness l is l= 1mm=0.001m, the diameter D is D=0.021m, so the cross section area is $A=\pi\cdot(D/2)^2=0.000346\ m^2$.

In the tunneling equation $\left[\frac{2\alpha}{h^2}E\exp\left(-\frac{h\beta}{2r_pE}\right)+\frac{\sigma_f}{r_ph}\right]$, α and β are pre-exponential and exponential terms of the standard Fowler-Nordheim Tunneling which are both constants. In this case, value α is set as 2, value β is set as 1. h is the height of the RVU as two times of iron particle's radius. So h=0.000004 m. The iron particle's radius r_p is 0.000002 m. σ_f is the conductivity of the polymer film namely silicone rubber. Because of the high resistance of silicone rubber, the value of conductivity of silicone rubber σ_f is set as $1*10^{-10}$. The electric field E is from the function file of the multimeter used in the test. The value of E is 9V. So the whole equation can be calculated as $\frac{2\alpha}{h^2}E\exp\left(-\frac{h\beta}{2r_pE}\right)+\frac{\sigma_f}{r_ph}\approx 2.01*10^{12}$. At the normal condition, the MRE Young's modulus E_p is set as 4000 Pa. The Poisson's ratio of particles ν is set as 0.1. Substitute these parameters into Equation (9), the final resistance of Gr-MREs is

$$R_g=\frac{4.78*10^{-13}\times\lambda_g\lambda_i}{10^{-8}+0.000002\left(\left(2000+\sigma_1+\sigma_2\right)^{1/3}-2000^{1/3}\right)\times 0.001166} \tag{10}$$

where σ_1 is the compressive stress from the external force and σ_2 is the compressive stress from the external magnetic field [25]. In this study, the weight of plastic plate is 10 g and the weight increment is 110 g. Thus, the force increment is 1 N. The stress, σ_1, is then calculated by dividing the force with the area A (0.000346 m^2), and shown in Table 2.

External load(N)	Real load(N)	Compressive stress σ_1 (Pa)
0	0.1	288.7165
1	1.1	3175.881
2	2.1	6063.045
3	3.1	8950.21
4	4.1	11837.37
5	5.1	14724.54
6	6.1	17611.7
7	7.1	20498.87
8	8.1	23386.03
9	9.1	26273.2
10	10.1	29160.36

Table 2. Relation of weight, load and compressive stress

The anisotropic MRE with graphite weight fraction 21.95% (contains 10g iron particles, 3g silicone rubber, 3g silicone oil and 4.5g graphite powder) can be used as an example. Table 3 shows the volume fractions of all the ingredients for this sample.

	Mass(g)	Density(g/cm^3)	volume(cm^3)	Volume fraction
Iron particle	10	7.86	1.272265	16.50%
Silicone rubber	3	3.18	0.943396	12.24%
Silicone oil	3	0.96	3.125	40.54%
Graphite powder	4.5	1.9	2.368421	30.72%

Table 3. Volume fractions of all the ingredients (anisotropic MRE Gr 21.95%)

The factors showing the efforts of graphite and iron particles to the resistance in Gr-MREs are λ_g and λ_i respectively and λ_g and λ_i depend on the graphite volume fraction ϕ_g and iron particles volume fraction ϕ_i . For each sample there are different values for λ_g and λ_i. Fig. 25 shows the product of λ_g and λ_i versus Gr-MREs (Gr 20%, 21.95% and 23.81%). The data is from the ratio of experimental result and theoretical prediction.

If we set $\lambda_g = \exp(a \cdot \phi_g)$ and $\lambda_i = \exp(b \cdot \phi_i)$ and substitute the data in Table 4 and Fig. 8 to λ_g and λ_i, the parameters λ_g and λ_i can be obtained and so the parameter a and b were derived as -65 and 250, respectively. So the relationship of λ_g and λ_i to ϕ_g and ϕ_i are $\lambda_g = e^{-65*\varphi_g}$, $\lambda_i = e^{250\varphi_i}$

	Gr 20%	Gr 21.95%	Gr 23.81%
Iron particle (ϕi)	17.09%	16.5%	15.96%
Graphite powder(ϕg)	28.27%	30.7%	33.01%

Table 4. Volume fractions of iron and graphite (anisotropic MRE Gr 20%, 21.95% & 23.81%)

After having determined all parameters, Equation 10 is ready to calculate the final resistance R_g of the anisotropic MRE with graphite weight fraction 20%.

5.2.2. Comparison and analysis

To show the comparison between the experimental result and the theoretical prediction, anisotropic MRE with graphite weight fraction 21.95% is considered. Comparison between experimental and theoretical result is provided in Fig. 26.

Figure 26 shows that the experimental and theoretical result do not match each other perfectly. However, the trends of both experimental result and theoretical result are the same.

Similarly some other comparison can be made from the data. At the fixed external force (which is expressed as load) when the magnetic field intensity increases the resistance of the

sample decreases. The data under three external loads such as 1 N, 5 N and 10 N were chosen to compare the experimental and theoretical result in Fig. 27.

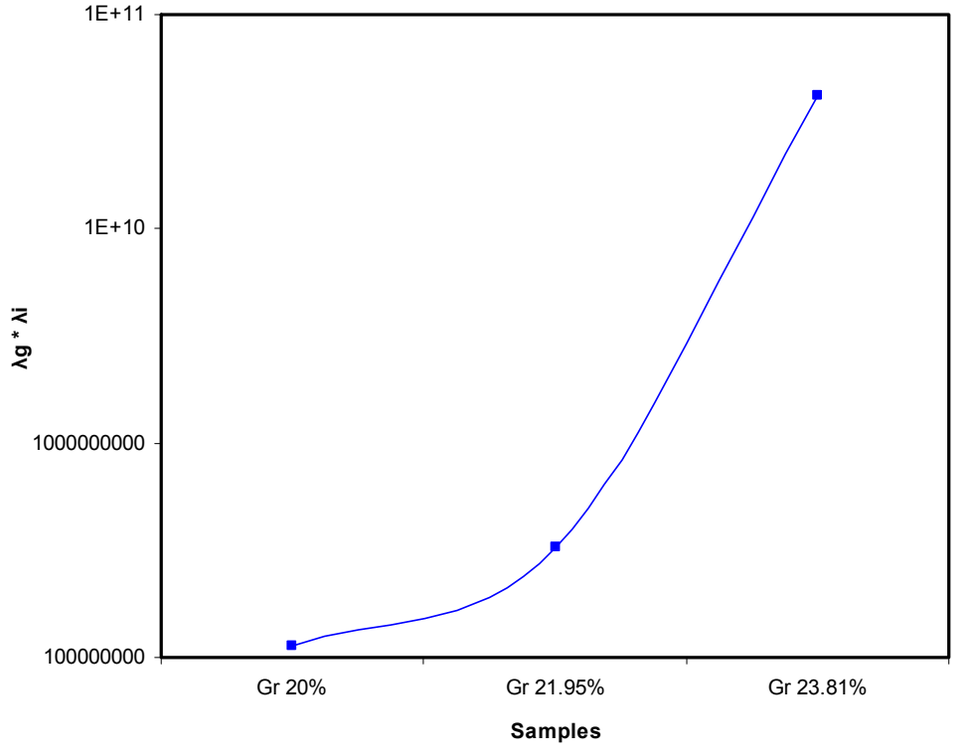

Figure 25. $\lambda_g * \lambda_i$ versus graphite weight fraction

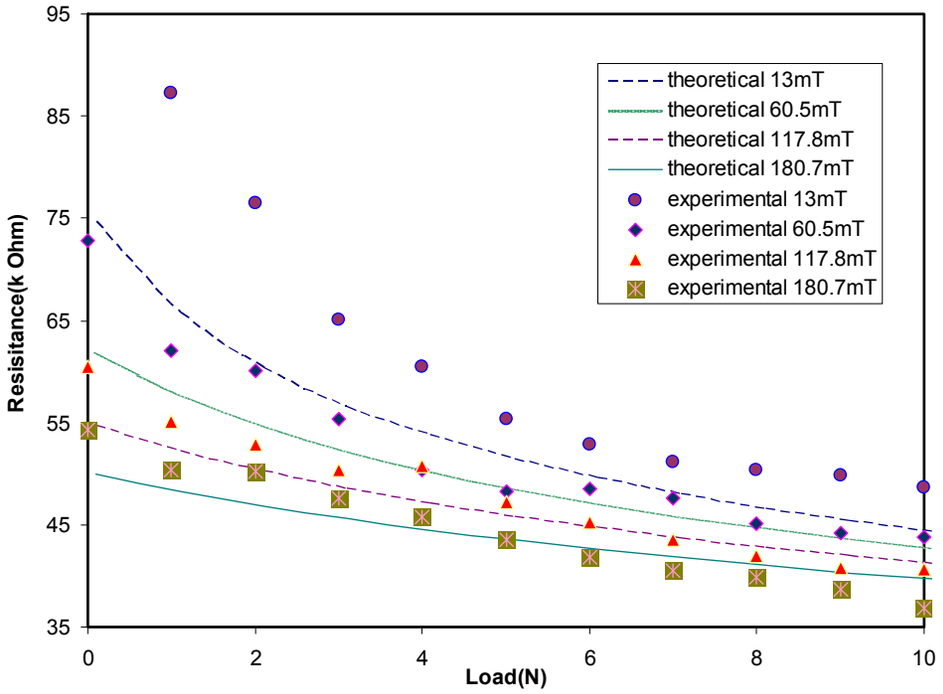

Figure 26. Comparison between experimental result and theoretical result (anisotropic MRE Gr 21.95%)

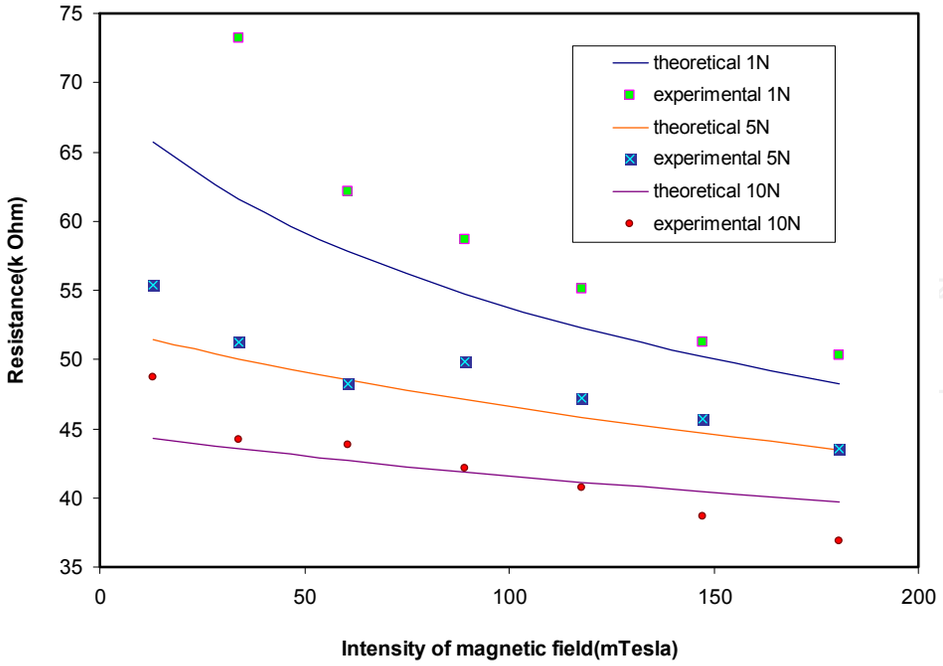

Figure 27. Resistance changing at a fixed load (anisotropic MRE Gr 21.95%)

The Fig. 27 shows the change in the resistance for given external forces. Along with the raising of magnetic field intensity, the sample's resistance decreases. The higher external load applied leads to lower resistance of Gr-MREs.

The next two figures Fig. 28 and 29 show the resistance variation between anisotropic MREs with graphite weight fraction 20%, 21.95%, and 23.81%. The magnetic field is fixed in Fig. 28 and the external load is fixed in Fig. 29.

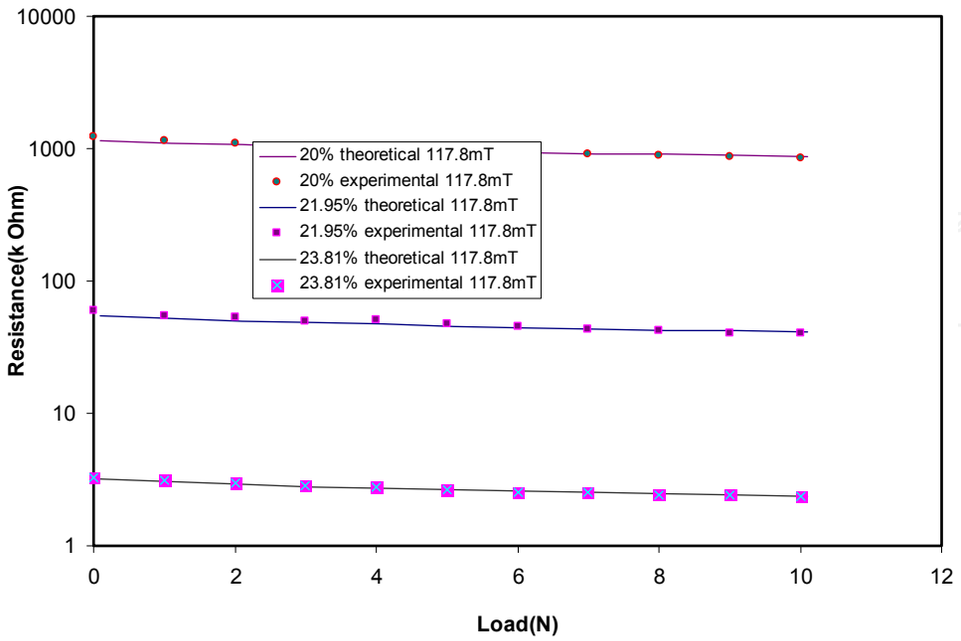

Figure 28. Resistance between different sample at 117.8mT magnetic field (anisotropic MRE with graphite weight fraction 20%, 21.95% & 23.81%

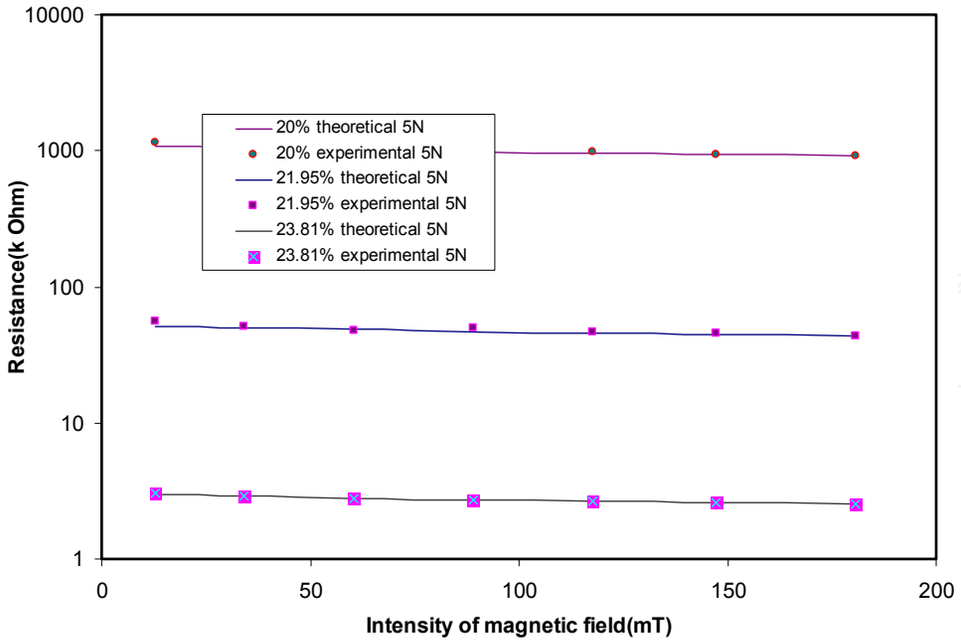

Figure 29. Resistance between different samples at 5.1N external load (anisotropic MRE with graphite weight fraction 20%, 21.95% & 23.81%)

Because of the order of values for the three samples it is easy to see from the Fig. 28 and 29 that theoretical and experimental results can match each other very well. This again provides a proof of the theory and when either external load or magnetic field intensity increases the resistance decrease.

Therefore when the magnetic field intensity and resistance are measured, Equation 10 can be used to calculate the value of the external load which means the Gr-MREs have the potential to work as the key component in a force sensor.

6. Conclusion

Both isotropic and anisotropic samples of graphite-based magnetorheological elastomers (Gr-MREs) with various graphite weight fractions ranging from 0% to 23.8% were fabricated in this study. The microstructural observation of these samples shows that the presence of graphite powder affects the forming of carbonyl iron chains. The sample with less graphite shows better-aligned carbonyl iron chains which influence the magnetorheology of MREs. In addition by connecting two iron chains in parallel and connecting the disconnected iron chains, the graphite contributes to the conductivity of MREs.

Steady state and dynamic tests such as strain amplitude sweep and angular frequency sweep were used to test the magnetorheology of Gr-MREs. With the help of graphite in MREs, the Storage and Loss Moduli are both changed. The steady state tests showed that the graphite can diminish the viscoelastic linear range of MREs. The dynamic tests proved that the samples with higher graphite weight fraction show higher initial Storage and Loss Moduli and lower MR effects. Additionally, the resistance of each MRE sample exhibits a decreasing trend with the graphite weight fraction.

Based on a Dipole model, a representative volume unit was presented to show the resistance of ideal anisotropic MREs. The current flowing through the ideal chain structure were derived by taking into account both the tunnel current and conductivity current. In the mathematical model, two parameters, λ_i and λ_g, were introduced to reflect the effect of the iron particles and graphite, which are both exponential functions of particle volume fractions. The exponential parameters were identified and then used to reconstruct modelling predictions. The comparison between experimental results with modelling predictions indicate that the proposed mathematical model can well investigate the sensing capabilities of the graphite based MRE elastomers.

Author details

Weihua Li and Tongfei Tian
School of Mechanical, Materials & Mechatronic Engineering, University of Wollongong, Wollongong, NSW, Australia

Haiping Du
School of Electrical, Computer and Telecommunications Engineering, Wollongong, NSW, Australia

Acknowledgement

This work is partially supported by the University of Wollongong through a UIC funding scheme.

7. References

[1] G. Y. Zhou and Z. J. Jiang, "Deformation in magnetorheological elastomer and elastomer-ferromagnet composite driven by a magnetic field", *Smart Mater. Struct.*, 13: 309-316 (2004)

[2] X. L. Gong, X. Z. Zhang and P. Q. Zhang, "Fabrication and Characterization of Isotropic Magnetorheological Elastomers", *Polymer Testing*, 24(5): 669–676 (2005)

[3] H. X. Deng, X. L. Gong and L. H. Wang, "Development of an adaptive tuned vibration absorber with magnetorheological elastomer", *Smart Materials & Structures*, 15 (5): N111-N116 (2006)

[4] Zou, H., Zhang, L.Q., Tian, M., Wu, S.Z. and Zhao, S.H., 2009. Study on the Structure and Properties of Conductive Silicone Rubber Filled with Nickel-Coated Graphite. Journal of Applied Polymer Science, 115(5): p. 2710-2717.

[5] Li, W.H., Kostidis, K., Zhang, X.Z., Zhou, Y. and Ieee. 2009. 'Development of a Force Sensor Working with MR Elastomers'. in 2009 Ieee/Asme International Conference on Advanced Intelligent Mechatronics, Vols 1-3. New York: Ieee.

[6] Ginder, J.M., Clark, S.M., Schlotter, W.F. and Nichols, M.E., 2002. Magnetostrictive phenomena in magnetorheological elastomers. International Journal of Modern Physics B, 16(17-18): p. 2412-2418.

[7] Lokander, M. and Stenberg, B., 2003. Performance of isotropic magnetorheological rubber materials. Polymer Testing, 22(3): p. 245-251.
[8] Lokander, M. and Stenberg, B., 2003. Improving the magnetorheological effect in isotropic magnetorheological rubber materials. Polymer Testing, 22(6): p. 677-680.
[9] Zhou, G.Y., 2003. Shear properties of a magnetorheological elastomer. Smart Materials and Structures, 12(1): p. 139.
[10] Ginder, J.M., Schlotter, W.F. and Nichols, M.E. 2001. 'Magnetorheological elastomers in tunable vibration absorbers'. in Smart Structures and Materials 2001: Damping and Isolation. Newport Beach, CA, USA: SPIE.
[11] Gong, X.L., Zhang, X.Z. and Zhang, P.Q., 2005. Fabrication and characterization of isotropic magnetorheological elastomers. Polymer Testing, 24(5): p. 669-676.
[12] Kchit, N. and Bossis, G., 2009. Electrical resistivity mechanism in magnetorheological elastomer. Journal of Physics D-Applied Physics, 42(10): p. 5505-5505.
[13] Wang, X.J., Gordaninejad, F., Calgar, M., Liu, Y.M., Sutrisno, J. and Fuchs, A., 2009. Sensing Behavior of Magnetorheological Elastomers. Journal of Mechanical Design, 131(9): p. 6.
[14] Bica, I., 2009. Influence of the transverse magnetic field intensity upon the electric resistance of the magnetorheological elastomer containing graphite microparticles. Materials Letters, 63(26): p. 2230-2232.
[15] Li, W.H., Kostidis, K., Zhang, X.Z., Zhou, Y. and Ieee, Development of a Force Sensor Working with MR Elastomers, in 2009 Ieee/Asme International Conference on Advanced Intelligent Mechatronics, Vols 1-3. 2009, Ieee: New York. p. 233-238.
[16] Zhao, Y., Maietta, D.M. and Chang, L., 2000. An Asperity Microcontact Model Incorporating the Transition From Elastic Deformation to Fully Plastic Flow. Journal of Tribology, 122(1): p. 86-93.
[17] McLachlan, D.S., 2000. Analytical functions for the dc and ac conductivity of conductor-insulator composites. Journal of Electroceramics, 5(2): p. 93-110.
[18] Woo, L.Y., Wansom, S., Hixson, A.D., Campo, M.A. and Mason, T.O., 2003. A universal equivalent circuit model for the impedance response of composites. Journal of Materials Science, 38(10): p. 2265-2270.
[19] Weinberg, Z.A., 1982. On tunneling in metal-oxide-silicon structures. Journal of Applied Physics, 53(7): p. 5052-5056.
[20] Serdouk, S., Hayn, R. and Autran, J.L., 2007. Theory of spin-dependent tunneling current in ferromagnetic metal-oxide-silicon structures. Journal of Applied Physics, 102(11): p. 113707-1-113707-5.
[21] Dahlke, W.E. and Sze, S.M., 1967. Tunneling in metal-oxide-silicon structures. Solid State Electronics, 10(8): p. 865-873.
[22] Zhupanska, O.I. and Ulitko, A.F., 2005. Contact with friction of a rigid cylinder with an elastic half-space. Journal of the Mechanics and Physics of Solids, 53(5): p. 975-999.
[23] Etsion, I., Levinson, O., Halperin, G. and Varenberg, M., 2005. Experimental investigation of the elastic-plastic contact area and static friction of a sphere on flat. Journal of Tribology, 127(1): p. 47-50.

[24] Maouche, N., Maitournam, M.H. and Dang Van, K., 1997. On a new method of evaluation of the inelastic state due to moving contacts. Wear, 203-204: p. 139-147.
[25] Chang, W.R., Etsion, I. and Bogy, D.B., 1988. Static Friction Coefficient Model for Metallic Rough Surfaces. Journal of Tribology, 110(1): p. 57-63.

IntechOpen